duced into T cells. Here, we successfully transferred the cDNA library to a lentivirus vector and found that CD14 can confer resistance to HIV-induced cell death in the transduced cells. This observation suggests that the transferred libraries can still be applied for a functional screening system. Because the vector has also been used to transduce genes into nondividing cells such as neurons (11, 12), muscles (7), and hematopoietic stem cells (4), our lentivirus-based system can be applied to expression cloning systems that use such cells.

However, there is a need to improve our library transfer system. Some degree of loss in library complexity was noted. In our experiment, some of the cDNAs, especially long cDNA fragments, appeared to be lost during two steps: PCR amplification and lentivirus vector production and/or infection. This problem would be solved when the long cDNA fragments are enriched before the BP reaction and a genetic library is directly generated on a donor vector for the LR reaction. We think the latter strategy is useful because, if a library is constructed on a donor vector, the library can be transferred to various expression vector systems, which include not only the lentivirus vector but also other traditional vector systems, by only the LR reaction. As shown in Table 1, we did not observe the loss of library complexity during the LR reaction in our experiment. To overcome the loss of parts of the long cDNA fragments during production of lentivirus vector and/or infection, shorter parent lentiviral vector DNAs should be used in future experiments. In the present study, we used a GFP-expressing lentivirus vector DNA (CSII-EF-MCS-IRES-hrGFP). To obtain long cDNA inserts in the lentiviral vector, there is probably a need to delete some parts of the fragment within the vector DNA, such as IRES-hrGFP.

It was reported that the lentivirus (derived from HIV-1) vector-transduced T cells are less susceptible to wild-type HIV-1 infection than nontransduced T cells (3). The transcripts transduced by the vector appears to compete efficiently for encapsidation, resulting in inhibition of its infectivity, probably because *cis*-acting sequences in the lentivirus vector are responsive to the regulatory protein of wild-type HIV-1. However, the inhibitory effect was completely eliminated in a self-inactivating vector (3). Thus, we used a self-inactivating vector, and we could not actually find any differences in its HIV-1 replication ability between the transduced and nontransduced cells (data not shown).

In the present study, we used a cDNA library as a functional genetic element. In the future, we will be able to choose different genetic libraries, such as ribozyme (8) and peptide libraries (23, 25). The ribozyme library can be efficiently expressed under the control of an RNA polymerase III-dependent promoter (8). When constructing a lentivirus vector containing such a library, the Gateway-based transfer system will be useful. Moreover, since the length of such a library is more homogeneous and shorter than a conventional cDNA library, the lentivirus vector system will be able to more potently deliver a ribozyme library than a cDNA library.

CD14 is known as a coreceptor molecule for lipopolysaccharide (LPS) (24) and is expressed on the surface of myeloid cells via a glycosylphosphatidyl inositol tail. LPS binds to a serum protein, LPS-binding protein (15), and associates with CD14. Subsequently, LPS stimulates Toll-like receptor 4 (13) and activates signaling pathways, mainly the nuclear factor-κB (NF-κB) pathway. HIV-1 also preferentially infects macrophages that express CD14. It is known that macrophages are one of the major target cells for HIV infection, and they behave as cellular reservoirs of virions in HIV-infected patients, probably because the cells are relatively resistant to HIV-induced CPE (5). Although the mechanisms of the low susceptibility of macrophages to HIV-1-induced cell death are poorly understood at present, some explanations may be brought up from the resistance of CD14-transduced cells to HIV-1-induced cell death. One explanation is that overexpression of CD14 can trigger cell survival signals such as NF-κB or induce antiapoptotic genes. Another explanation is that CD14 can reduce the cytotoxicity of HIV-1 infection in T cells through a partial inhibition of HIV-1 replication. In fact, CD14 overexpression resulted in an inhibition of the entry step on HIV-1 replication, as shown in Fig. 5. A determination of the exact mechanisms of CD14 function in HIV-infected cells should enhance our understanding of the cellular events during HIV-induced cell death, which results in immune destruction in HIV-infected individuals.

In conclusion, application of the Gateway system to a genetic library transfer system will allow the use of the lentivirus vector system as a powerful tool for the study of functional genomics of mammalian cells.

ACKNOWLEDGMENTS

We thank I. Verma for providing several reagents used in our study.

This work was supported by a Grant-in-Aid for Scientific Research on Priority Areas from the Ministry of Education, Culture, Sports, Sciences, and Technology of Japan; by grants for Research on HIV-AIDS and Health Science from the Ministry of Health, Labor, and Welfare of Japan. Y. Koyanagi was also supported by a grant from the Naito Foundation.

REFERENCES

1. **Aruffo, A., and B. Seed.** 1987. Molecular cloning of a CD28 cDNA by a high-efficiency COS cell expression system. Proc. Natl. Acad. Sci. USA **84**: 8573–8577.
2. **Aruffo, A., and B. Seed.** 1987. Molecular cloning of two CD7 (T-cell leukemia antigen) cDNAs by a COS cell expression system. EMBO J. **6**:3313–3316.
3. **Bukovsky, A. A., J. P. Song, and L. Naldini.** 1999. Interaction of human immunodeficiency virus-derived vectors with wild-type virus in transduced cells. J. Virol. **73**:7087–7092.
4. **Case, S. S., M. A. Price, C. T. Jordan, X. J. Yu, L. Wang, G. Bauer, D. L. Haas, D. Xu, R. Stripecke, L. Naldini, D. B. Kohn, and G. M. Crooks.** 1999. Stable transduction of quiescent $CD34^+CD38^-$ human hematopoietic cells by HIV-1-based lentiviral vectors. Proc. Natl. Acad. Sci. USA **96**:2988–2993.
5. **Gartner, S., P. Markovits, D. M. Markovitz, M. H. Kaplan, R. C. Gallo, and M. Popovic.** 1986. The role of mononuclear phagocytes in HTLV-III/LAV infection. Science **233**:215–219.
6. **Hachiya, A., S. Aizawa-Matsuoka, M. Tanaka, Y. Takahashi, S. Ida, H. Gatanaga, Y. Hirabayashi, A. Kojima, M. Tatsumi, and S. Oka.** 2001. Rapid and simple phenotypic assay for drug susceptibility of human immunodeficiency virus type 1 using CCR5-expressing HeLa/$CD4^+$ cell clone 1-10 (MAGIC-5). Antimicrob. Agents Chemother. **45**:495–501.
7. **Kafri, T., U. Blomer, D. A. Peterson, F. H. Gage, and I. M. Verma.** 1997. Sustained expression of genes delivered directly into liver and muscle by lentiviral vectors. Nat. Genet. **17**:314–317.
8. **Ko, M. S. H.** 2001. Embryogenomics: developmental biology meets genomics. Trends Biotechnol. **19**:511–518.
9. **Kuwata, H., Y. Watanabe, H. Miyoshi, M. Yamamoto, T. Kaisho, K. Takeda, and S. Akira.** 2003. IL-10-inducible Bcl-3 negatively regulates LPS-induced TNF-α production in macrophages. Blood **102**:4123–4129.
10. **Miyoshi, H., K. A. Smith, D. E. Mosier, I. M. Verma, and B. E. Torbett.** 1999. Transduction of human $CD34^+$ cells that mediate long-term engraftment of NOD/SCID mice by HIV vectors. Science **283**:682–686.
11. **Naldini, L., U. Blomer, F. H. Gage, D. Trono, and I. M. Verma.** 1996. Efficient transfer, integration, and sustained long-term expression of the transgene in adult rat brains injected with a lentiviral vector. Proc. Natl. Acad. Sci. USA **93**:11382–11388.

12. **Naldini, L., U. Blomer, P. Gallay, D. Ory, R. Mulligan, F. H. Gage, I. M. Verma, and D. Trono.** 1996. In vivo gene delivery and stable transduction of nondividing cells by a lentiviral vector. Science 272:263–267.
13. **Poltorak, A., X. He, I. Smirnova, M.-Y. Liu, C. V. Huffel, X. Du, D. Birdwell, E. Alejos, M. Silva, C. Galanos, M. Freudenberg, P. Ricciardi-Castagnoli, B. Layton, and B. Beutler.** 1998. Defective LPS signaling in C3H/HeJ and C57BL/10ScCr mice: mutations in Tlr4 gene. Science 282:2085–2088.
14. **Reboul, J., P. Vaglio, N. Tzellas, N. Thierry-Mieg, T. Moore, C. Jackson, T. Shin-i, Y. Kohara, D. Thierry-Mieg, J. Thierry-Mieg, H. Lee, J. Hitti, L. Doucette-Stamm, J. L. Hartley, G. F. Temple, M. A. Brasch, J. Vandenhaute, P. E. Lamesch, D. E. Hill, and M. Vidal.** 2001. Open-reading-frame sequence tags (OSTs) support the existence of at least 17,300 genes in C. elegans. Nat. Genet. 27:332–336.
15. **Schumann, R. R., S. R. Leong, G. W. Flaggs, P. W. Gray, S. D. Wright, J. C. Mathison, P. S. Tobias, and R. J. Ulevitch.** 1990. Structure and function of lipopolysaccharide binding protein. Science 249:1429–1431.
16. **Seed, B.** 1995. Developments in expression cloning. Curr. Opin. Biotechnol. 6:567–573.
17. **Seed, B., and A. Aruffo.** 1987. Molecular cloning of the CD2 antigen, the T-cell erythrocyte receptor, by a rapid immunoselection procedure. Proc. Natl. Acad. Sci. USA 84:3365–3369.
18. **Shevchenko, Y., G. G. Bouffard, Y. S. Butterfield, R. W. Blakesley, J. L. Hartley, A. C. Young, M. A. Marra, S. J. Jones, J. W. Touchman, and E. D. Green.** 2002. Systematic sequencing of cDNA clones using the transposon Tn5. Nucleic Acids Res. 30:2469–2477.
19. **Simpson, J. C., V. E. Neubrand, S. Wiemann, and R. Pepperkok.** 2001. Illuminating the human genome. Histochem. Cell Biol. 115:23–29.
20. **Suzuki, Y., N. Misawa, C. Sato, H. Ebina, T. Masuda, N. Yamamoto, and Y. Koyanagi.** 2003. Quantitative analysis of human immunodeficiency virus type 1 DNA dynamics by real-time PCR: integration efficiency in stimulated and unstimulated peripheral blood mononuclear cells. Virus Genes 27:177–188.
21. **van Maanen, M., J. K. Tidwell, L. A. Donehower, and R. E. Sutton.** 2003. Development of an HIV-based cDNA expression cloning system. Mol. Ther. 8:167–173.
22. **Walhout, A. J. N. M., R. Sordella, X. Lu, J. L. Hartley, G. F. Temple, M. A. Brasch, N. Thierry-Mieg, and M. Vidal.** 2000. Protein interaction mapping in C. elegans using proteins involved in vulval development. Science 287:116–122.
23. **Welch, P. J., E. G. Marcusson, Q.-X. Li, C. Beger, M. Kruger, C. Zhou, M. Leavitt, F. Wong-Staal, and J. R. Barber.** 2000. Identification and validation of a gene involved in anchorage-independent cell growth control using a library of randomized hairpin ribozymes. Genomics 66:274–283.
24. **Wright, S. D., R. A. Ramos, P. S. Tobias, R. J. Ulevitch, and J. C. Mathison.** 1990. CD14, a receptor for complexes of lipopolysaccharide (LPS) and LPS binding protein. Science 249:1431–1433.
25. **Xu, X., C. Leo, Y. Jang, E. Chan, D. Padilla, B. C. Huang, T. Lin, T. Gururaja, Y. Hitoshi, J. B. Lorens, D. C. Anderson, B. Sikic, Y. Luo, D. G. Payan, and G. P. Nolan.** 2001. Dominant effector genetics in mammalian cells. Nat. Genet. 27:23–29.

European Journal of Neuroscience, Vol. 20, pp. 2499–2508, 2004

Intrinsic and spontaneous neurogenesis in the postnatal slice culture of rat hippocampus

Maki Kamada,[1] Ren-Yong Li,[1] Mika Hashimoto,[2] Masaaki Kakuda,[1,2] Hiroshi Okada,[3] Yoshio Koyanagi,[4] Toru Ishizuka[1,2] and Hiromu Yawo[1,2]
[1]CREST, JST, Kawaguchi 332–0012, Japan
[2]Department of Developmental Biology and Neurosciences, Tohoku University Graduate School of Life Sciences, 2–1 Seiryo-machi, Aoba-ku, Sendai 980–8575, Japan
[3]Department of Virology, Tohoku University Graduate School of Medicine, Sendai 980–8575, Japan
[4]Laboratory of Viral Pathogenesis, Institute for Virus Research, Kyoto University, Kyoto 606–8507, Japan

Keywords: adult neurogenesis, calbindin, dentate gyrus, enhanced green fluorescent protein, virus

Abstract

Organotypic slice culture preserves the morphological and physiological features of the hippocampus of live animals for a certain time. The hippocampus is one of exceptional regions where neurons are generated intrinsically and spontaneously throughout postnatal life. We investigated the possibility that neurons are generated continuously at the dentate granule cell layer (GCL) in slice culture of the rat hippocampus. Using 5-bromodeoxyuridine (BrdU) labelling and retrovirus vector transduction methods, the phenotypes of the newly generated cells were identified immunohistochemically. At 4 weeks after BrdU exposure, BrdU-labelled cells were found in the GCL and were immunoreactive with a neuronal marker, anti-NeuN. There were fibrils immunoreactive with anti-glial fibrillary acidic protein (GFAP), an astrocyte marker, in the layer covering the GCL and occasionally encapsulated BrdU-labelled nuclei. When the newly divided cells were marked with the enhanced green fluorescent protein (EGFP) using a retrovirus vector, these cells had proliferative abilities throughout the following 4-week cultivation period. Four weeks after the inoculation, the EGFP-expressing cells consisted of various phenotypes of both early and late stages of differentiation; some were NeuN-positive cells with appearances of neurons in the GCL and some were immunoreactive with anti-Tuj1, a marker of immature neurons. Some EGFP-expressing cells were immunoreactive with anti-GFAP or anti-nestin, a marker of neural progenitors. The present study suggests that slice cultures intrinsically retain spontaneous neurogenic abilities for their cultivation period. The combination of slice culture and retrovirus transduction methods enable the newly divided cells to be followed up for a long period.

Introduction

In the mammalian central nervous system, the hippocampus is one of regions where new neurons are generated intrinsically and spontaneously throughout the postnatal life of animals (Altman & Das, 1965; Cameron *et al.*, 1993; Gould *et al.*, 1999b; Kornack & Rakic, 1999) including humans (Eriksson *et al.*, 1998). These cells acquire neuron-like appearances with axons and dendrites (van Praag *et al.*, 2002), neuron-specific marker proteins such as NeuN and Tuj1 (Cameron *et al.*, 1993; Eriksson *et al.*, 1998; Kornack & Rakic, 1999; van Praag *et al.*, 2002) and neuron-like membrane properties such as action potentials and synaptic potentials (van Praag *et al.*, 2002) during the course of maturation. Moreover, these cells migrate to be integrated in the dentate granule cell layer (GCL), express calbindin D28K, a GCL cell marker protein (Kuhn *et al.*, 1996; Eriksson *et al.*, 1998) and project axons into the CA3 region (Hastings & Gould, 1999; Markakis & Gage, 1999). Neural stem cells derived from the adult hippocampus differentiate into neuron-like cells and form synaptic networks *in vitro* (Song *et al.*, 2002). These morphological and physiological features strongly suggest that the new neurons would be incorporated in the hippocampal local circuitry and that they would be involved in hippocampus-dependent memory formation (Shors *et al.*, 2001; Kempermann, 2002; van Praag *et al.*, 2002) and brain repair (Gould & Tanapat, 1997; Liu *et al.*, 1998; Kuhn *et al.*, 2001).

Organotypic cultures of hippocampal slices would provide an alternative model to hippocampus *in vivo* (Gähwiler *et al.*, 1997). As all types of neurons and glia are preserved with their specific morphologies and localizations in hippocampal slice cultures, the main network organization is very similar to that of living animals (Gähwiler, 1984; Zimmer & Gähwiler, 1984; Dailey *et al.*, 1994). However, a few rearrangements have been observed probably as a result of afferent deprivation (Robain *et al.*, 1994; Gutierrez & Heinemann, 1999). Neurons in slice culture maintained their physiological membrane properties and synaptic transmissions as well as several forms of short- and long-term plasticity (Gähwiler *et al.*, 1997). Therefore, slice cultures have been used widely in studies on physiology, pharmacology, morphology and the plasticity of the hippocampus.

It is plausible that hippocampal slice cultures have potencies to generate new neurons *in vitro* as suggested by the observations that neural progenitor-like cells are found in the slice culture (Miyaguchi, 1997) and transplanted ES cells differentiate into neurons (Benninger

Correspondence: Dr Hiromu Yawo, [2]Department of Developmental Biology and Neurosciences, as above.
E-mail: yawo@mail.tains.tohoku.ac.jp

Received 28 June 2004, revised 26 August 2004, accepted 30 August 2004

doi:10.1111/j.1460-9568.2004.03721.x

et al., 2003). The presence of neurogenic abilities has recently been reported in hippocampal slice cultures by 5-bromodeoxyuridine (BrdU) labelling methods (Raineteau *et al.*, 2004). In the present study the newly generated cells were also identified by retrovirus vector transduction methods. We found that hippocampal slice cultures retain endogenous neural progenitors in the dentate gyrus throughout the cultivation period and maintain *per se* the potential to differentiate spontaneously into neurons. We followed up the newly generated cells for a long period and found that some newly generated neurons are indeed incorporated into the normal architecture of GCL with the expression of one of the GCL cell markers, calbindin D28K.

Materials and methods

Slice culture

Hippocampal organotypic cultures were prepared according to the standard interface method (Stoppini *et al.*, 1991; Sakaguchi *et al.*, 1994). Hippocampal slices were prepared from postnatal day 7 Wistar rats (Nihon SLC Co., Japan). After decapitation, the brain was removed and transversely sliced at the hippocampus into a 350 μm thickness on a McIlwain tissue chopper (The Mickle Laboratory Engineering, UK). The isolated hippocampal slices were transferred onto a porous translucent membrane (Millicell-CM: PICM03050, Millipore, Billerica, MA, USA) and maintained in culture at 34 °C for several weeks in the interface between culture medium and a 5% CO_2 atmosphere. The culture medium in this experiment was a mixture of 50% commercial medium (OPTI-MEM, Invitrogen, Carlsbad, CA, USA), 25% heat inactivated horse serum (Invitrogen) and 25% Hank's balanced salt solution (Invitrogen) supplemented with D-glucose (5 g/L), penicillin (100 units/mL; Invitrogen) and streptomycin (100 μg/mL; Invitrogen), and was changed twice a week. Slices were also prepared from an adult female Wistar rat, as a control. The animal was deeply anaesthetized with diethyl ether then decapitated. The brain was removed and hippocampal slices (100 μm thickness) were prepared. All of the animal treatments used here were performed in accordance with the guidelines laid down by the Japan Neuroscience Society and NIH.

To label the immediately post-mitotic cells, slices at 13–14 days *in vitro* (DIV) were incubated for 3 days with culture medium containing 10 μM 5-bromodeoxyuridine (BrdU, Roche Diagnostics, Indianapolis, IN, USA) and then to normal medium. One to four weeks after BrdU treatment, the slices were fixed with 4% paraformaldehyde in 0.1 M sodium phosphate buffer for 1 h at 4 °C.

Retrovirus vector transduction

A murine leukaemia virus-based vector, SRαLEGFP (An *et al.*, 1999), was derived from SRα*Lthy* (An *et al.*, 1997) by replacing the murine thy1.2 gene with enhanced green fluorescent protein (EGFP). Vector stocks were generated by calcium phosphate-mediated transfection of HEK 293T cells. HEK 293T cells were cultured in Dulbecco's modified Eagle medium with 10% calf serum, 100 units/mL penicillin and 100 μg/mL streptomycin in a 5% CO_2 incubator and transfected the following day with the envelope plasmid pMD.G (Zufferey *et al.*, 1997), the packaging plasmid pSVψ-E-murine leukaemia virus (Landau & Littman, 1992) and the transfer vector plasmid SRαLEGFP. At 24 h post-transfection, the medium was replaced with serum-free medium (OPTI-MEM; Invitrogen). At 48 h post-transfection, the virus-containing supernatant was collected, centrifuged and passed through a 0.45 μm filter. The virus vectors were further concentrated by centrifugation at 6000 *g* for 16 h at 4 °C. The pellet was resuspended in serum-free medium and kept in liquid nitrogen until use. Stocks of the vector were titrated by infecting NIH3T3 cells and analysing for EGFP expression by flow cytometry. The titre of vectors was 5×10^5 infectious units/mL.

Slices at 14 DIV were inoculated with the retrovirus vector encoding EGFP in the suprapyramidal region of the GCL. Then, 2–4 weeks later, the slices were fixed with 4% paraformaldehyde in 0.1 M sodium phosphate buffer for 1 h at 4 °C and used for immunohistochemical studies.

Zinc histofluorescence

The distribution of axons (mossy fibres; MFs) and their terminals in GCL neurons was investigated using a membrane-permeable zinc-sensitive fluorescent indicator, *N*-(6-methoxy-8-quinolyl)-*p*-toluenesulphonamide (TSQ, Molecular Probes, Eugene, OR, USA). TSQ (5 mg) was dissolved in 333 μL dimethyl sulphoxide (DMSO) containing 20% pluronic acid (Dojindo Laboratories, Kumamoto, Japan) and stored at 4 °C. A TSQ solution (1 : 250) was freshly prepared by adding Ca^{2+}-free Tyrode's solution, which reduced the release probability and thereby prevented translocation of the zinc from presynaptic terminals. The vital or freshly frozen slices at 2–6 weeks *in vitro* (WIV) were immersed in the TSQ solution for 30 min at 34 °C and briefly rinsed in Tyrode's solution containing EDTA disodium-calcium salt (Ca-EDTA, 10 mM) to chelate extracellular free zinc (Varea *et al.*, 2001). The slices were finally viewed by using a conventional epifluorescence microscope (BX51, Olympus, Tokyo, Japan) equipped with a WU excitation/detection filter and recorded using a digital camera system (PDMC-II, Polaroid, Cambridge, MA, USA).

Immunohistochemistry

The slices were fixed with 4% paraformaldehyde in 0.1 M sodium phosphate buffer at 4 °C for 1 h, then washed in PBS. For BrdU detection, the slices were incubated in 2 N HCl at 37 °C for 1 h to denature DNA, neutralized twice with 0.1 M borate buffer (pH 8.5) for 30 min and washed twice in PBS. After peeling the slices off from the membrane, all the subsequent procedures were carried out on free-floating slices using a rotator. The slices were blocked in PBS with 5% normal goat serum and 0.3% Triton X-100 at 4 °C overnight and reacted with the following primary antibodies in phosphate-buffered saline (PBS) with 5% normal goat serum and 0.3% Triton X-100 at 4 °C for 24 h: mouse monoclonal anti-NeuN (1 : 1000; Chemicon, Temecula, CA, USA), mouse monoclonal anti-βIII tubulin (Tuj1; 1 : 1000; Promega, Madison, WI, USA), mouse monoclonal anti-MAP2 (1 : 1000; Sigma-Aldrich, St Louis, MO, USA), mouse monoclonal anti-nestin (1 : 1000; Chemicon), guinea pig polyclonal anti-GFAP (1 : 1000; Advanced Immunochemical, Long Beach, CA, USA), rabbit polyclonal anti-GFAP (1 : 1000; Promega), rat monoclonal anti-BrdU [Clone:BU1/75 (ICR1); 1 : 100; Oxford Biotechnology, UK] or rabbit polyclonal anti-EGFP produced by Tamamaki *et al.* (2000) (1 : 500; a generous gift from Dr Y. Yanagawa, Gunma University, Japan). The preparations were then washed three times in PBS with 0.1% Triton X-100 and incubated at room temperature for 5–6 h with fluorescent dye conjugated secondary antibodies (each, 1 : 200) from different species: Alexa Fluor 546-conjugated anti-mouse IgG; Alexa Fluor 488-conjugated anti-guinea pig IgG; Alexa Fluor 488-, 546- or 633-conjugated anti-rat IgG; and Oregon Green 488-conjugated anti-rabbit IgG (all purchased from Molecular Probes). To ensure that our labelling patterns were not the conse-

quence of a dye artifact, double or triple immunolabelling was performed sequentially. After washing three times in PBS with 0.1% Triton X-100, the slices were mounted with Permafluor (Immunotech, France). Each specimen was analysed three-dimensionally with a z-axis interval of 0.87–0.88 μm under a conventional confocal laser microscope (LSM510META, Zeiss, Thornwood, NY, USA) equipped with 40 × objectives unless otherwise noted. The images were corrected for brightness and contrast using conventional software (LSM Image Browser version 3.2, Zeiss and Photoshop version 6.0, Adobe Systems Inc, San Jose, CA, USA).

Results

Cellular architecture of granule cell layer

Hippocampal slices prepared from postnatal rats were cultured for several weeks. The gross appearances of slices between 2 and 6 weeks of plating (Fig. 1, A2 and A3) were similar to those from the living intact animal (Fig. 1, A1) as noted in the previous studies (Stoppini *et al.*, 1991; Okada *et al.*, 1995). To further investigate the cellular architecture of the slice culture, neurons were identified by the expression of neuronal nuclei antigen (NeuN), which is expressed specifically in the nucleus of mature neuron with unknown functions (Mullen *et al.*, 1992). Similar to the living animal (Fig. 1, B1), GCL cells and pyramidal cell layer (PCL) cells of the CA1–4 region were preserved for as long as 6 WIV (Fig. 1, B2 and B3). The GCL was usually compact and clearly discriminated from the surrounding tissues in the suprapyramidal region whereas neurons formed a loose cluster and occasionally migrated out from the slices in the infrapyramidal region (e.g. Fig. 1, B2). To identify the GCL, all the following experiments were limited to the suprapyramidal region.

Next, we investigated whether the laminar arrangement of the slice culture assures optimal hippocampal networks. In the hippocampus *in vivo* the MF gives rise to fine collaterals with numerous small boutons in the hilus and traverses the apical dendritic shafts of CA3 pyramidal cells in a narrow band called the stratum lucidum (Henze *et al.*, 2000). Presynaptic boutons of the MF contain an exceptionally high concentration of zinc in the synaptic vesicles (Frederickson *et al.*, 2000). To identify the MF projection we applied a zinc sensitive fluorescent indicator, TSQ, which brightly

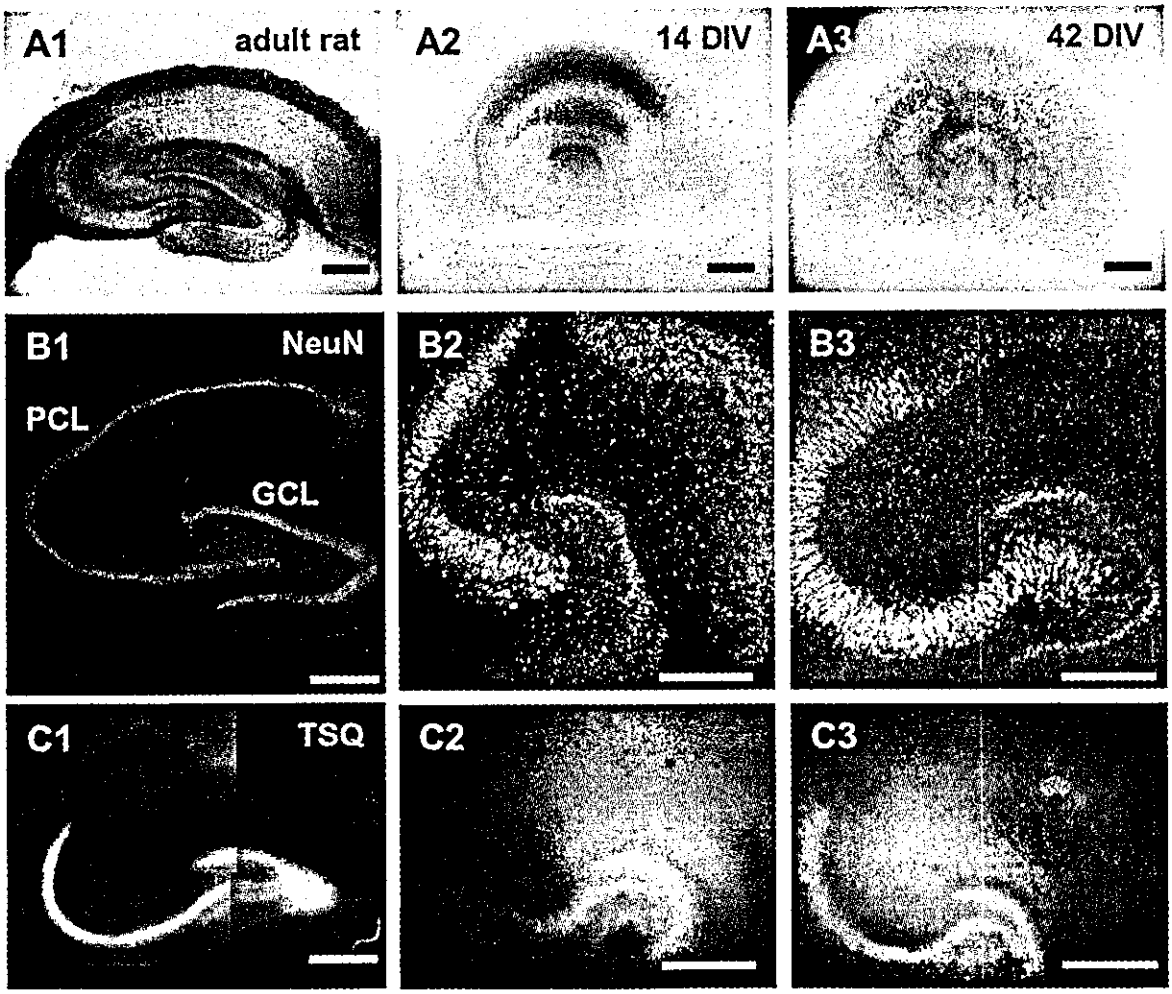

FIG. 1. The cellular architecture of rat hippocampal slice cultures. (A1–3) Plain views of hippocampal slice and its culture: the acute slice from an adult rat (A1), 14 DIV slice culture (A2) and 42 DIV slice culture (A3). (B1–3) The organizations of neuronal layers: the acute slice from adult rat (B1), 14 DIV slice culture (B2) and 42 DIV slice culture (B3). Neurons were immunolabelled with anti-NeuN, a neuron-specific marker. Note the presence of both the dentate granule cell layers (GCLs) and the CA1–4 pyramidal cell layers (PCLs). (C1–3) The laminar arrangements of mossy fibre (MF) projections: the acute slice from adult rat (C1), 14 DIV slice culture (C2) and 42 DIV slice culture (C3). The MFs and their terminals were visualized with a zinc-sensitive fluorescent indicator, *N*-(6-methoxy-8-quinolyl)-*p*-toluenesulphonamide (TSQ). The pattern of MF projections in the slice cultures is similar to that *in vivo*. Scale bars, 0.5 mm.

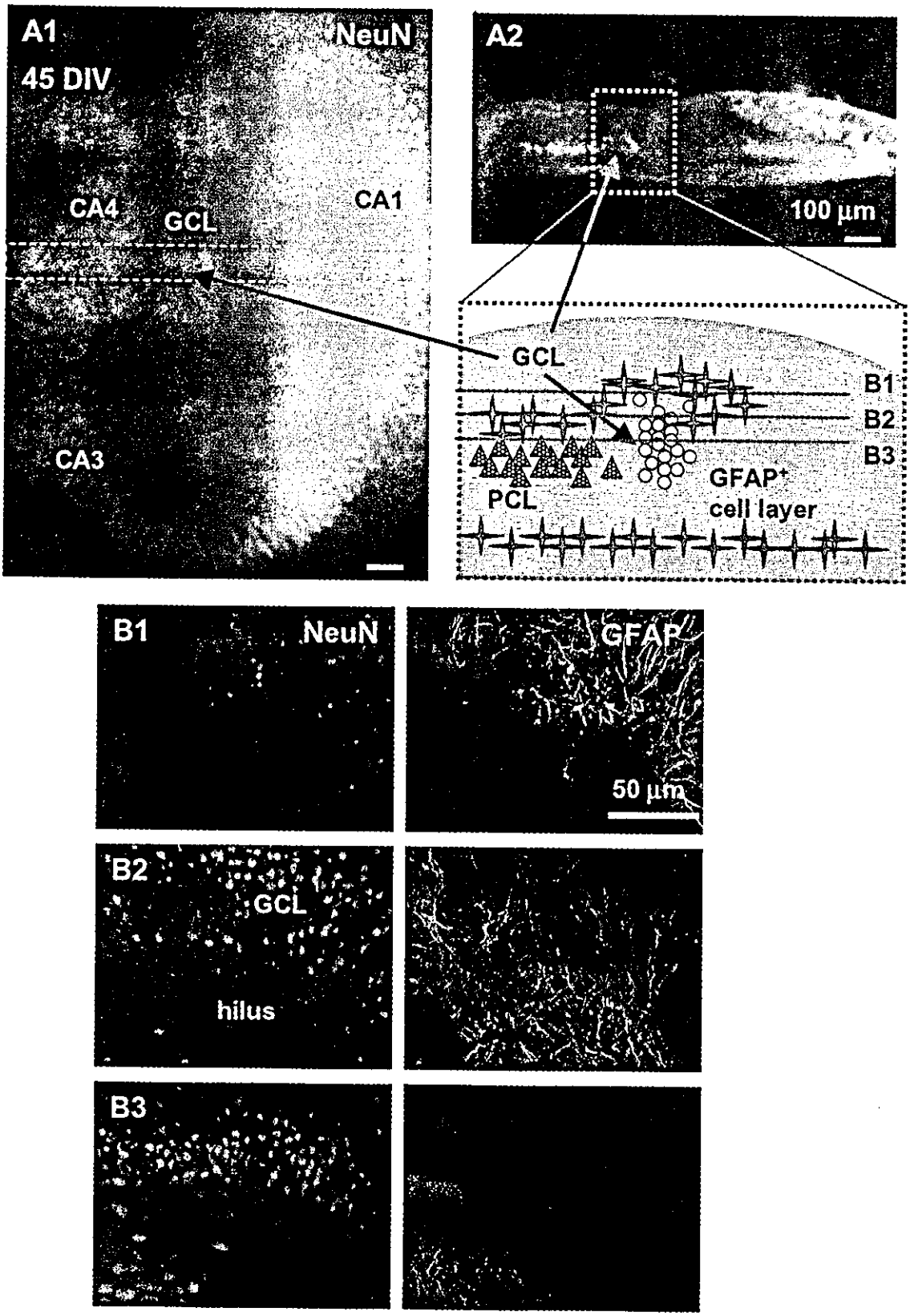

FIG. 2. Three-dimensional architecture of the dentate gyrus. (A1 and 2) The distribution of neurons in a 45 DIV slice culture: the horizontal (A1) and vertical (A2) appearances. Neurons were immunolabelled with anti-NeuN. The region between broken lines in A1 is viewed from the side in A2. The cartoon of cytoarchitecture corresponds to the square region in A2. The dotted lines, B1–3 correspond to the following panels B1–3, respectively. Neurons in the GCL and PCL are indicated by circles and triangles, respectively, and astrocytes by stars. The unidentified structure of slice culture is coloured in grey. (B1–3) The three-dimensional distribution of neurons and astrocytes in the dentate gyrus of a slice culture 6 μm above the layer of GCL (B1), the layer where GCL first appears (B2) and 6 μm below B2 (B3). The double immunofluorescent images of anti-NeuN (left), anti-GFAP (right) were obtained by using confocal microcopy.

labels the following regions (Fig. 1, C1): hilus of dentate gyrus; CA3 suprapyramidal and infrapyramidal layer. These brightly fluorescent regions were almost identical to those obtained with other metal-histochemical methods like Timm staining method (Frederickson *et al.*, 1987; Vogt *et al.*, 2000). Throughout the cultivation period TSQ brightly labelled these regions in some slices: 40.0% ($n = 25$) at 14 DIV (Fig. 1, C2); and 31.5% ($n = 108$) at 42 DIV (Fig. 1, C3). However, MF projections were obscure in others, probably through the massive reorganization of axonal trajectories or the ectopic projections in slice cultures (Robain *et al.*, 1994; Gutierrez & Heinemann, 1999). As the presence of robust MF projections is an indication of the preservation of efficient hippocampal architecture, all the following experiments were carried out after TSQ identification of MF projections.

Three-dimensional architecture of the dentate gyrus

Even when hippocampal slice cultures had preserved laminar structures for several weeks, the slices were flattened within the first week and maintained their thickness for subsequent weeks, as reported previously (Buchs *et al.*, 1993). To determine the position and thickness of the GCL in the slice culture, slices at 45 DIV were cut in a perpendicular plane to the Millicell-CM membrane along the CA1–4 axis, which had been previously fixed and immunolabelled for anti-NeuN (Fig. 2, A1). Slices had thinned to 179 ± 12 μm ($n = 11$; Fig. 2, A2) from the previous thickness of 350 μm. The PCL was stretched horizontally at CA1, as reported previously (Buchs *et al.*, 1993), whereas the GCL (thickness of tens of micrometres) was buried in the middle of the slice and was densely packed with neurons with small-sized nuclei.

To resolve the three-dimensional cytoarchitecture of the dentate gyrus, the culture slices at 45 DIV were immunolabelled with anti-NeuN and anti-glial fibrillary acidic protein (GFAP), specific antibodies to one of intermediate filament proteins and one of selective markers of astrocytes and radial glia (Ludwin *et al.*, 1976; Seri *et al.*, 2001), and inspected by using confocal laser scanning microscopy from the surface to the bottom (see Fig. 2 cartoon). There was a layer of GFAP-positive cells just above the GCL (Fig. 2, B1). In the layer containing the GCL, there was a dense cluster of NeuN-positive small nuclei, surrounded by GFAP-positive cells (Fig. 2, B2). In the deeper layer, NeuN-positive cells were found in the GCL as well as the PCL at CA4 (Fig. 2, B3). Although we did not determine the type of cells located under the neuronal somatic area, GFAP-positive processes sometimes tightly formed a thin layer in a vicinity of the Millicell-CM membrane.

Differentiation of endogenous progenitors in slice cultures

To investigate whether endogenous progenitors exist intrinsically and actually differentiate into neurons in the slice culture, we added BrdU, a thymidine analogue, to the culture medium. As BrdU is incorporated into nuclei during the S-phase, it should label the newly generated cells in slice cultures. The phenotype of BrdU-labelled cells was identified immunohistochemically using antibodies to neuronal or glial markers, under higher magnification. Usually, the suprapyramidal region of the GCL was set in the centre of the optical field, and the optical planes above and in the GCL were examined. In the case of slices at 45 DIV, triple immunofluorescent labelling (anti-BrdU, anti-NeuN and anti-GFAP) was carried out to identify the specific phenotypes of BrdU-labelled cells.

One week after BrdU treatment, many BrdU-labelled cells were found in and around the GCL, and occasionally appeared as pairs being opposed each other (Fig. 3, B1 and B3, arrowheads), but were coexpressed with neither NeuN (Fig. 3, A1–3) nor microtubule-associated protein 2 (MAP2; Fig. 3, B1–3), one of the cytoskeletal proteins expressed specifically in neuronal cell bodies and dendrites (Bernhardt & Matus, 1984). Many of these BrdU-labelled nuclei did not associate with GFAP-positive structures overlaying the GCL (Fig. 3, C1-3). However, under close inspection of three-dimensional structures, a few BrdU-labelled nuclei were encapsulated by the GFAP-positive fibres (asterisk). Some BrdU- and GFAP-positive cells had characteristic short processes (Fig. 3C, insets). These BrdU-labelled cells might also include non-neuronal and non-glial cells as microglia and fibroblasts although both cells are supposed to be few in the region around the GCL (Raineteau *et al.*, 2004).

Four weeks after treatment, confocal images revealed that some of the BrdU-labelled nuclei were coexpressed with NeuN in the GCL (Fig. 4, A1–3, arrowheads). These cells were not immunoreactive with anti-GFAP (Fig. 4, A4). The coexpression of BrdU and NeuN was examined three-dimensionally under higher magnification (Fig. 4B). In the layer overlaying the GCL, there were some BrdU-labelled nuclei surrounded by GFAP-positive processes (Fig. 4, C1–3, arrows). These cells were not immunolabelled by anti-NeuN (Fig. 4, C4).

Visualization of endogenous neurogenesis in living slices

The BrdU-labelling method has several disadvantages for the study of neurogenesis. Neurogenesis is only retrospectively identified in fixed tissues. Labelling with BrdU is not sufficient to prove that a given cell has divided because BrdU is a marker of DNA synthesis rather than of cell division (Rakic, 2002). BrdU-labelling alone does not reveal morphological characteristics of the newly generated cells as BrdU is incorporated into only their nuclei. Finally, the cellular and physiological features of living cells are difficult to investigate. To overcome these disadvantages, we marked endogenous progenitors in living slice cultures with EGFPs using retrovirus vectors, which were injected locally into the suprapyramidal region of the GCL. As the retroviruses infect only dividing cells and their genes are incorporated into the host's genomic DNA, newly divided cells and their descendants would specifically express EGFP.

From daily observations of the injected sites under fluorescent microscopy, the EGFP-expressing cells showed a tendency to increase in number between 1- and 2-weeks post-inoculation (Fig. 5, A1 and A2). The number of EGFP-expressing cells was followed up in six slices in which more than four EGFP-expressing cells were identified in the DGL 1 week after retrovirus vector inoculation and was even increased in the next 1–3 weeks (Fig. 5B). The relative number increased to 253 ± 58% (mean ± SEM; $n = 5$) in 1 week and to 296 ± 104% ($n = 4$) in 2 weeks. As our retrovirus vector is replication-incompetent, the EGFP-expressing cells proliferated as a result of mitosis. In the first 1–2-weeks post-inoculation, the typical EGFP-expressing cells were small with short processes (Fig. 5A), being reminiscent of the undifferentiated cells that had recently appeared. Indeed, three-dimensional analysis of confocal images revealed that 36 ± 4% (mean ± SEM; four slices, sum of double positive cells/total EGFP-expressing cells = 45/128) of these cells expressed nestin, one of intermediate filaments expressed specifically in neuroblasts and myoblasts (Lendahl *et al.*, 1990) and a putative neural precursor markers (see also Fig. S1 in Supplementary material). By contrast, the EGFP-expressing cells have neither neuronal appearances nor detectable NeuN immunoreactivities in these early

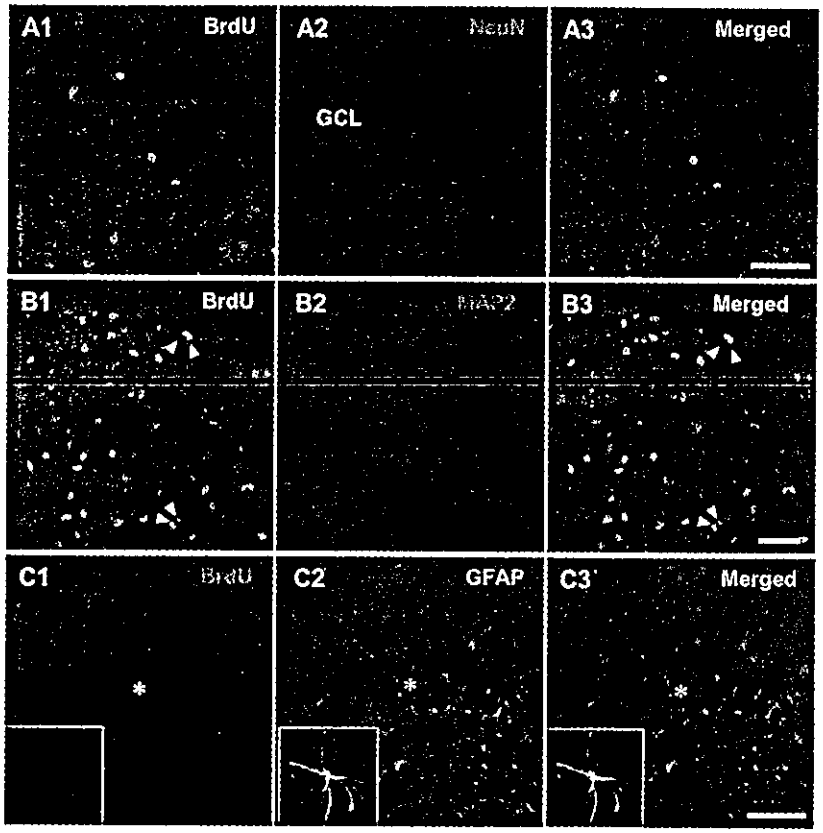
A1
BrdU
A2
NeuN
GCL
A3
Merged
B1
BrdU
B2
MAP2
B3
Merged
C1
BrdU
C2
GFAP
C3'
Merged

FIG. 3.

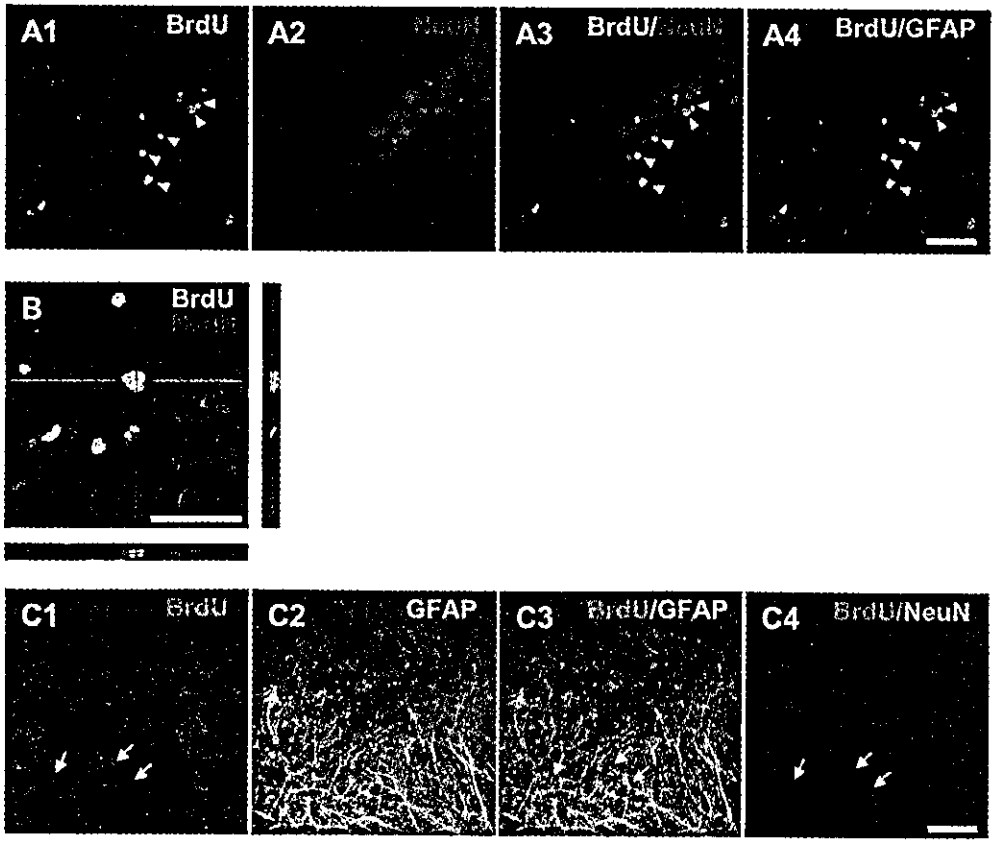
A1
BrdU
A2
A3
BrdU/
A4
BrdU/GFAP
B
BrdU
C1
BrdU
C2
GFAP
C3
BrdU/GFAP
C4
BrdU/NeuN

FIG. 4.

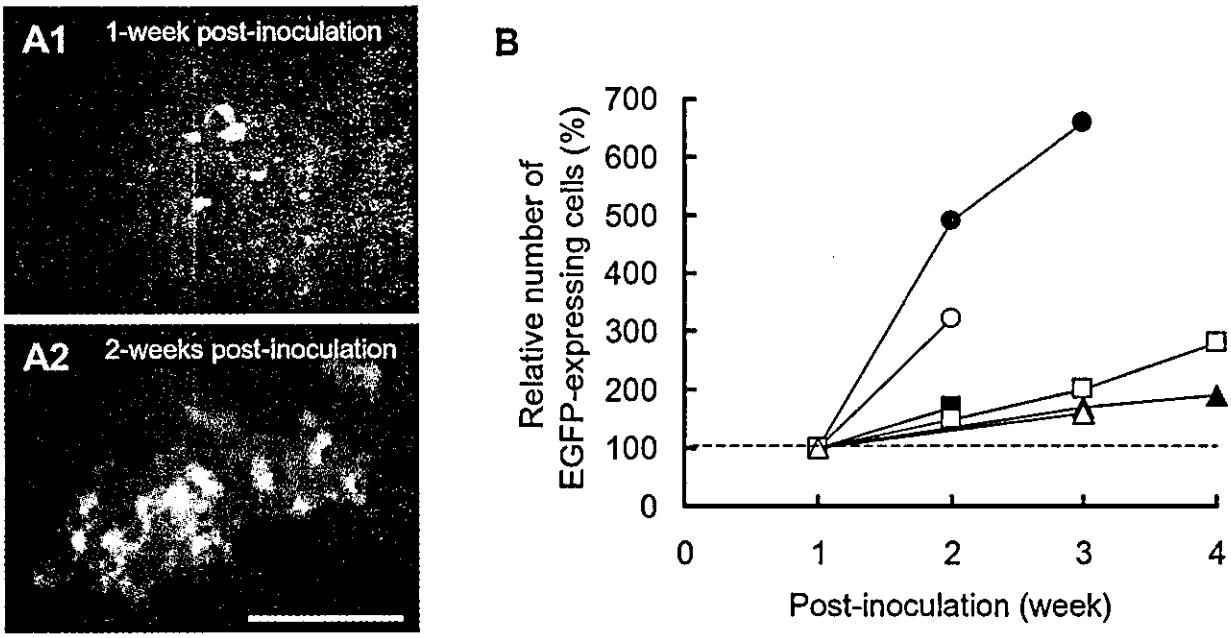

FIG. 5. Proliferation of enhanced green fluorescent protein (EGFP)-expressing cells after retrovirus vector inoculation. (A) The EGFP-expressing cells in the dentate gyrus at 1- (A1) and 2-weeks (A2) post-inoculation in the same place. Scale bar, 50 μm. (B) The number of EGFP-labelled cells in the dentate gyrus was counted, normalized to that seen at 1-week postinoculation and plotted against time. Each symbol represents an identical slice culture ($n = 6$).

postinoculation periods, indicating that our retrovirus vectors would not transfect mature neurons.

Some of the EGFP-expressing cells extended processes in the late WIV

Three-dimensional analysis of confocal images were investigated for phenotypes of EGFP-expressing cells 4 weeks after inoculation. Typical EGFP-expressing cells were seen in the GCL with several dendrite-like processes (Fig. 6A) and one elongated axon-like process (Fig. 6A, arrowheads) bearing putative synaptic boutons (Fig. 6A, arrow). The coexpression of EGFP and NeuN (Fig. 6B) was examined three-dimensionally under higher magnification (Fig. 6C). Some of these cells were immunoreactive to anti-NeuN and were incorporated in the normal architecture of GCL (Fig. 6A and B). Some EGFP-expressing cells represented early phenotypes of differentiation into neurons in the GCL with short processes and immunolabelled with antibodies to Tuj1 (Fig. 6D), one of the cytoskeletal proteins expressed specifically in immature neurons (Lee *et al.*, 1990). The detailed morphology of neuron-like EGFP-expressing cells also varied, as shown in Fig. 6A and B. Some dendrite-like processes extended to z-axis directions whereas others were horizontal. Some axon-like processes extended in the direction of CA3 pyramidal cells whereas in others it was the opposite. We tracked these axons for a considerable length but were unable to find the final destinations. To test if these EGFP-expressing cells have phenotypes of GCL neurons, the coexpression of EGFP and calbindin D28K, one of calcium binding proteins expressed specifically in some types of neurons including DGL cells (Baimbridge & Miller, 1982; Bousez-Dumesnil *et al.*, 1989) was examined three-dimensionally under a higher magnification (Fig. 6E). Indeed, there were the neuron-like EGFP-expressing cells immunoreactive to calbindin D28K in the DGL. These results are consistent with the notion that the slice cultures intrinsically retain a neurogenic potential qualitatively similar to the hippocampus in the living animal.

To investigate the occurrence of neuronal differentiation, retrovirus vectors were injected on the same day in the same place of the suprapyramidal region of the DGL of 14 DIV slice cultures derived from 10 littermates of either gender and prepared on the same day. Four weeks after inoculation, 14 slice cultures were selected for analysis of phenotypes because they had numbers (> 10) of EGFP-expressing cells. The immunoreactivity to anti-NeuN was investigated

FIG. 3. Phenotypes of newly generated cells in the dentate gyrus one week after incorporation of 5-bromodeoxyuridine (BrdU). (A1–3) The double immunofluorescent confocal images of GCL: anti-BrdU (A1, green), anti-NeuN (A2, red) and the merge (A3). (B1–3) The double immunofluorescent confocal images of GCL: anti-BrdU (B1, green), anti-MAP2 (B2, red) and the merge of both (B3). The double arrowheads indicate mitotic figures. (C1–3) The double immunofluorescent confocal images of the dentate gyrus: anti-BrdU (C1, red), anti-GFAP (C2, green) and the merge (C3). The asterisk indicates the BrdU-labelled GFAP-positive cell. Inset shows another BrdU-labelled GFAP-positive cell with processes clearly visible. Scale bars, 50 μm.

FIG. 4. Phenotypes of newly generated cells in the dentate gyrus four weeks after incorporation of BrdU. (A1–4) The triple immunofluorescent confocal images of GCL: anti-BrdU (A1, green), anti-NeuN (A2, red), the merge of both (A3) and the merge of anti-BrdU and anti-GFAP (blue) images (A4). The arrowheads indicate the newly generated neurons which are both BrdU-labelled and NeuN-positive. (B) Three-dimensional confocal micrograph showing a typical BrdU/NeuN-immunoreactive cell. The x–z and y–z images were accompanied. Note that BrdU distributes in the nucleus of the NeuN-positive cell in the DGL. (C1–4) Triple immunofluorescent confocal images of the layer overlaying GCL: anti-BrdU (C1, red), anti-GFAP (C2, green), the merge (C3) and the merge of anti-BrdU and anti-NeuN (blue) images (C4). The arrows indicate the BrdU-labelled GFAP-positive cell. Scale bars, 50 μm.

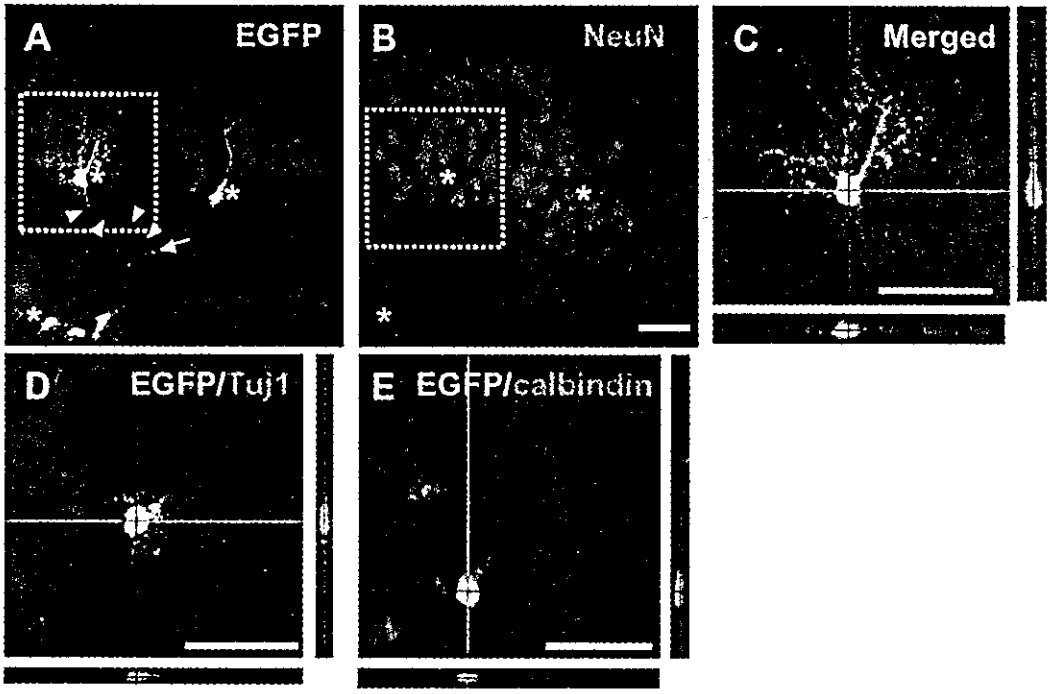

FIG. 6. Emergence of neuronal phenotypes in EGFP-expressing cells four weeks after retrovirus vector inoculation. (A and B) The double immunofluorescent confocal images of GCL: anti-EGFP (A, green), anti-NeuN (B, red). Typical EGFP-expressing NeuN-positive cells bear dendrite-like processes and an axon-like process (arrowheads) with a terminal bouton-like structure (arrow). EGFP-expressing cells that are immunoreactive with anti-NeuN are indicated by asterisks. (C) Three-dimensional analysis of a NeuN-positive EGFP-expressing cell. A rectangular region in A and B were merged and enlarged with x–z and y–z images. (D) Three-dimensional analysis of a double immunofluorescent confocal image of GCL: anti-EGFP (green) and anti-Tuj1 (red). The x–z and y–z images were accompanied. (E) Three-dimensional analysis of a double immunofluorescent confocal image of GCL: anti-EGFP (green); anti-calbindin D28K (red). The x–z and y–z images were accompanied. Scale bars, 50 μm.

in four slices. The NeuN-positive cells were found in the range of 10–40% of the EGFP-expressing cells. In total 23 of 91 EGFP-expressing cells were NeuN-positive (25%). The Tuj1-positive cells were in the range of 10–40% of the EGFP-expressing cells (four slices) and 23 of 94 EGFP-expressing cells in total (24%). Therefore, some but not all newly divided cells express neuronal phenotypes (see Fig. S1 in Supplementary material). In fact, in this series of experiments, the GFAP-positive cells were in the range of 10–40% of the EGFP-expressing cells (three slices) and 33 of 103 EGFP-expressing cells in total (32%). The nestin-positive cells were in the range of 10–40% of the EGFP-expressing cells (four slices) and 36 of 133 EGFP-expressing cells in total (27%).

Discussion

We made several observations reinforcing the previous study that postnatal hippocampal slice cultures preserve endogenous neuronal progenitor cells in the dentate gyrus, in which new neurons are spontaneously generated (Raineteau *et al.*, 2004). With BrdU used to label dividing cells, we found that some BrdU-labelled cells acquire phenotypes of mature neurons in the following four weeks. Using retrovirus vectors, we found that in 4 weeks some EGFP-expressing cells also acquire phenotypes of mature neurons extending dendrites and axon-like processes.

Differences between labelling methods

One of our new findings is that EGFP-expressing cells proliferated in the explanted hippocampus during the cultivation period between 1- and 4-week postinoculation (Fig. 5). This is in contrast to the observation that the number of BrdU-labelled cells has a tendency to decrease in days after early proliferation (Hayes & Nowakowski, 2002). Since BrdU is incorporated into DNA during mitosis, its density diminishes during the following cell divisions (Dayer *et al.*, 2003). Therefore, the descendents of highly proliferative cells would become negligible regarding BrdU immunoreactivity. Alternatively, the undifferentiated cells might be selected for survival before differentiation with massive cell death (Gould *et al.*, 1999a). Either way, it is generally accepted that BrdU preferentially labels the immediately post-mitotic cells during the period of drug exposure. By contrast, the retrovirus vector transduction reveals a different population of cells, the newly divided ones and their descendents.

Neurogensis in the slice culture system

In this study some BrdU-labelled cells in the GCL were also positive for NeuN, a marker of mature neurons (Fig. 4A and B). These observations are consistent with reports of *in vivo* preparations (Kuhn *et al.*, 1996; Eriksson *et al.*, 1998; Kornack & Rakic, 1999) and slice culture systems (Raineteau *et al.*, 2004), and imply that intrinsic neural progenitors are present in the hippocampal slice culture of 2 WIV and that some of their descendents differentiate into GCL neurons.

Four weeks after retrovirus vector inoculation, about one-quarter of EGFP-expressing cells were immunoreactive with anti-NeuN and about one-quarter with anti-Tuj1, a marker of immature neurons. These numbers compare with those in *in vivo* experiments: 2–25% for anti-NeuN and 15–30% for anti-Tuj1, although these values do depend on the

behavioural conditions of the mice (van Praag *et al.*, 2002). The EGFP-expressing NeuN-positive cells were found primarily in the GCL of the slice culture (Fig. 6A and B). Similarly, most of the BrdU-labelled NeuN-positive cells were found in the GCL, being consistent with the previous study (Raineteau *et al.*, 2004). Therefore, the newly generated neurons are distributed similarly to that reported in postnatal mammals *in vivo* (Kuhn *et al.*, 1996; Eriksson *et al.*, 1998; Kornack & Rakic, 1999). We also found that some EGFP-expressing cells were immunoreactive to calbindin D28K, a marker of GCL neurons (Fig. 6E), being consistent with the *in vivo* studies (Kuhn *et al.*, 1996).

In the adult rodent brain, neurogenic stem cells are present in the subgranular zone of the hippocampus and the newly generated neurons preferentially distribute close to the subgranular zone in the GCL *in vivo* (Cameron *et al.*, 1993; Alvarez-Buylla & Lim, 2004) and in the thin slice culture using the roller-tube methods (Raineteau *et al.*, 2004). However, in our rather thick slice culture system using the interface methods (Stoppini *et al.*, 1991) we found no particular patterns in the appearance of BrdU-labelled/EGFP-expressing NeuN-positive cells in the GCL. Therefore, the three-dimensional structure of the neurogenic niche appears to be somewhat reorganized in our slice culture system.

Undifferentiated cells

One week after mitosis the large number of BrdU-labelled cells appeared to be undifferentiated because they were coexpressing with neither neuronal markers such as NeuN and MAP2 nor astrocyte markers such as GFAP (Fig. 3). Four weeks after retrovirus vector inoculation the EGFP-expressing cells consisted of various phenotypes: NeuN-positive (Fig. 6C); Tuj1-positive (Fig. 6D); GFAP-positive; and nestin-positive (see Supplementary material). Immediately after mitosis the descendants express nestin, an intermediate filament protein found in neuroepithelial stem cells, but usually lose it within a week during maturation (Palmer *et al.*, 2000). Therefore, those nestin-postive EGFP-expressing cells may have a history of recent mitosis. Although we did not investigate phenotypes of nestin-negative EGFP-expressing cells, neuronal and glial progenitors, microglia, endothelial cells and fibroblasts would be included (Raineteau *et al.*, 2004).

Neurons have been shown to express Tuj1 early in differentiation (Lee *et al.*, 1990; Menezes & Luskin, 1994) whereas they express NeuN after maturation (Mullen *et al.*, 1992). Some of our EGFP-expressing neurons showed phenotypes of either early or late stages of differentiation. It is, therefore, possible that there are lineages of self-renewing neural precursor cells that are neurogenic (Palmer *et al.*, 1997) as a consequence of asymmetric cell division (Alvarez-Buylla *et al.*, 2001; Fishell & Kriegstein, 2003). Alternatively, neurons might remain undifferentiated for weeks, and become mature by triggering signals, e.g. synaptic contacts. It is also possible that some of newly generated cells undergo apotosis before maturation (Gould & Gross, 2002) although the EGFP-expressing cells have a tendency to increase in number as a whole as late as 4 weeks after transduction (Fig. 5). Careful follow up of a single pair of EGFP-expressing cells in the slice culture system would shed light on this problem.

Gliogenesis in the slice culture system

Some BrdU-labelled cells expressed GFAP, a molecular marker of astrocytes (Fig. 4C) and about one-third of the EGFP-expressing cells were also positive for GFAP 4 weeks after retrovirus vector inoculation (see Supplementary material). These observations are consistent with previous *in vivo* experiments that cells positive for both BrdU and GFAP are present in the dentate hilus–subgranular zone in the hippocampus (Kempermann *et al.*, 1997). However, the GFAP-positive cells encompass a diverse group of cells (Seri *et al.*, 2001) including terminally differentiated astrocytes (Goldman, 2003) and radial glial cells, which have neurogenic potential (Seri *et al.*, 2001). It has been also suggested that neural precursor cells generally have a history of expressing GFAP at least once (Seri *et al.*, 2001; Kronenberg *et al.*, 2003). Experiments using other molecular markers are necessary to further classify these GFAP-positive cells.

There remains another issue as to whether the GFAP-positive cells and the NeuN-positive cells derived from the same progenitor. This could be tested in our slice culture system by following up a single pair of EGFP-expressing cells using retrovirus vector transduction.

Concluding remarks

Two independent studies, ours and that of Raineteau *et al.* (2004) would make it unequivocal that endogenous neural progenitor cells are indeed present in the slice culture system and spontaneously generating new neurons postnatally. Using the retrovirus vector transduction method in combination, the slice culture system would enable follow up of the newly divided cells for a long period.

Supplementary material

The following supplementary material may be found on: http://www.blackwellpublishing.com/products/journals/suppmat/EJN/EJN3721/EJN3721sm.htm

Fig. S1. Emergence of non-neuronal phenotypes in EGFP-expressing cells in the dentate gyrus around the suprapyramidal region of the GCL after retrovirus vector inoculation.

Acknowledgements

We are grateful to H. Minami for technical assistance R. Araki and K. Miyazaki for helpful comments and to M. Ohara (Fukuoka) for language assistance.

Abbreviations

BrdU, 5-bromodeoxyuridine; DIV, days *in vitro*; EGFP, enhanced green fluorescent protein; GFAP, glial fibrillary acidic protein; GCL, granule cell layer; MAP2, microtubule-associated protein 2; MF, mossy fibre; NeuN, neuronal nuclei antigen; PCL, pyramidal cell layer; TSQ, *N*-(6-methoxy-8-quinolyl)-*p*-toluenesulphonamide; Tuj1, neuron-specific β-III tubulin; WIV, weeks *in vitro*.

References

Altman, J. & Das, G.D. (1965) Autoradiographic and histological evidence of postnatal hippocampal neurogenesis in rats. *J. Comp. Neurol.*, **124**, 319–336.

Alvarez-Buylla, A., Garcia-Verdugo, J.M. & Tramontin, A.D. (2001) A unified hypothesis on the lineage of neural stem cells. *Nat. Rev. Neurosci.*, **2**, 287–293.

Alvarez-Buylla, A. & Lim, D.A. (2004) For the long run: maintaining germinal niches in the adult brain. *Neuron*, **41**, 683–686.

An, D.S., Koyanagi, Y., Zhao, J.-Q., Akkina, R., Bristol, G., Yamamoto, N., Zack, J.A. & Chen, I.S.Y. (1997) High-efficiency transduction of human lymphoid progenitor cells and expression in differentiated T cells. *J. Virol.*, **71**, 1397–1404.

An, D.S., Morizono, K., Li, Q.X., Mao, S.H., Lu, S. & Chen, I.S. (1999) An inducible human immunodeficiency virus type 1 (HIV-1) vector which effectively suppresses HIV-1 replication. *J. Virol.*, **73**, 7671–7677.

Baimbridge, K.G. & Miller, J.J. (1982) Immunohistochemical localization of calcium-binding protein in the cerebellum, hippocampal formation and olfactory bulb of the rat. *Brain Res.*, **245**, 223–229.

Benninger, F., Beck, H., Wernig, M., Tucker, K.L., Brustle, O. & Scheffler, B. (2003) Functional integration of embryonic stem cell-derived neurons in hippocampal slice cultures. *J. Neurosci.*, **23**, 7075–7083.

Bernhardt, R. & Matus, A. (1984) Light and electron microscopic studies of the distribution of microtubule-associated protein 2 in rat brain: a difference between dendritic and axonal cytoskeletons. *J. Comp. Neurol.*, **226**, 203–221.

Bousez-Dumesnil, N., Thomasset, M. & Ben-Ari, Y. (1989) Calbindin-D28K in hippocampal organotypic cultures. *Brain Res.*, **486**, 165–169.

Buchs, P.-A., Stoppini, L. & Muller, D. (1993) Structural modification associated with synaptic development in area CA1 of rat hippocampal organotypic cultures. *Dev. Brain Res.*, **71**, 81–91.

Cameron, H.A., Woolley, C.S., McEwen, B.S. & Gould, E. (1993) Differentiation of newly born neurons and glia in the dentate gyrus of the adult rat. *Neuroscience*, **56**, 337–344.

Dailey, M.E., Buchanan, J., Bergles, D.E. & Smith, S.J. (1994) Mossy fiber growth and synaptogenesis in rat hippocampal slices in vitro. *J. Neurosci.*, **14**, 1060–1078.

Dayer, A.G., Ford, A.A., Cleaver, K.M., Yassaee, M. & Cameron, H.A. (2003) Short-term and long-term survival of new neurons in the rat dentate gyrus. *J. Comp. Neurol.*, **460**, 563–572.

Eriksson, P.S., Perfilieva, E., Bjork-Eriksson, T., Alborn, A.-M., Nordborg, C., Peterson, D.A. & Gage, F.H. (1998) Neurogenesis in the adult human hippocampus. *Nat. Med.*, **4**, 1313–1317.

Fishell, G. & Kriegstein, A.R. (2003) Neurons from radial glia: the consequences of asymmetric inheritance. *Curr. Opin. Neurobiol.*, **13**, 34–41.

Frederickson, C.J., Kasarskis, E.J., Ringo, D. & Frederickson, R.E. (1987) A quinoline fluorescence method for visualizing and assaying the histochemically reactive zinc (bouton zinc) in the brain. *J. Neurosci. Meth.*, **20**, 91–103.

Frederickson, C.J., Suh, S.W., Silva, D., Frederickson, C.J. & Thompson, R.B. (2000) Importance of zinc in the central nervous system: the zinc-containing neuron. *J. Nutr.*, **130** (suppl.), 1471S–1483S.

Gähwiler, B.H. (1984) Development of the hippocampus in vitro: cell types, synapses and receptors. *Neuroscience*, **11**, 751–760.

Gähwiler, B.H., Capogna, M., Debanne, D., McKinney, R.A. & Thompson, S.M. (1997) Organotypic slice cultures: a technique has come of age. *Trends Neurosci.*, **20**, 471–477.

Goldman, S. (2003) Glia as neural progenitor cells. *Trends Neurosci.*, **26**, 590–596.

Gould, E., Beylin, A., Tanapat, P., Reeves, A. & Shors, T.J. (1999a) Learning enhances adult neurogenesis in the hippocampal formation. *Nat. Neurosci.*, **2**, 260–265.

Gould, E. & Gross, D.G. (2002) Neurogenesis in adult mammals: some progress and problems. *J. Neurosci.*, **22**, 619–623.

Gould, E., Reeves, A.J., Fallah, M., Tanapat, P. & Gross, C.G. (1999b) Hippocampal neurogenesis in adult Old World primates. *Proc. Natl. Acad. Sci. USA*, **96**, 5263–5267.

Gould, E. & Tanapat, P. (1997) Lesion-induced proliferation of neuronal progenitors in the dentate gyrus of the adult rat. *Neuroscience*, **80**, 427–436.

Gutierrez, R. & Heinemann, U. (1999) Synaptic reorganization in explanted cultures of rat hippocampus. *Brain Res.*, **815**, 304–316.

Hastings, N.B. & Gould, E. (1999) Rapid extension of axons into the CA3 region by adult-generated granule cells. *J. Comp. Neurol.*, **413**, 146–154.

Hayes, N.L. & Nowakowski, R.S. (2002) Dynamics of cell proliferation in the adult dentate gyrus of two inbred strains of mice. *Dev. Brain Res.*, **134**, 77–85.

Henze, D.A., Urban, N.N. & Barrionuevo, G. (2000) The multifarious hippocampal mossy fiber pathway: a review. *Neuroscience*, **98**, 407–427.

Kempermann, G. (2002) Why new neurons? Possible functions for adult hippocampal neurogenesis. *J. Neurosci.*, **22**, 635–638.

Kempermann, G., Kuhn, H.G. & Gage, F.H. (1997) More hippocampal neurons in adult mice living in an enriched environment. *Nature*, **386**, 493–495.

Kornack, D.R. & Rakic, P. (1999) Continuation of neurogenesis in the hippocampus of the adult macaque monkey. *Proc. Natl. Acad. Sci. USA*, **96**, 5768–5773.

Kronenberg, G., Reuter, K., Steiner, B., Brandt, M.D., Jessberger, S., Yamaguchi, M. & Kempermann, G. (2003) Subpopulations of proliferating cells of the adult hippocampus respond differently to physiologic neurogenic stimuli. *J. Comp. Neurol.*, **467**, 455–463.

Kuhn, H.G., Dickinson-Anson, H. & Gage, F.H. (1996) Neurogenesis in the dentate gyrus of the adult rat: age-related decrease of neuronal progenitor proliferation. *J. Neurosci.*, **16**, 2027–2033.

Kuhn, H.G., Palmer, T.D. & Fuchs, E. (2001) Adult neurogenesis: a compensatory mechanism for neuronal damage. *Eur. Arch. Psychiatry Clin. Neurosci.*, **251**, 152–158.

Landau, N.R. & Littman, D.R. (1992) Packaging system for rapid production of murine leukemia virus vectors with variable tropism. *J. Virol.*, **66**, 5110–5113.

Lee, M.K., Rebhun, L.I. & Frankfurter, A. (1990) Posttranslational modification of class III beta-tubulin. *Proc. Natl. Acad. Sci. USA*, **87**, 7195–7199.

Lendahl, U., Zimmerman, L.B. & McKay, R.D. (1990) CNS stem cells express a new class of intermediate filament protein. *Cell*, **60**, 585–595.

Liu, J., Solway, K., Messing, R.O. & Sharp, F.R. (1998) Increased neurogenesis in the dentate gyrus after transient global ischemia in gerbils. *J. Neurosci.*, **18**, 7768–7778.

Ludwin, S.K., Kosek, J.C. & Eng, L.F. (1976) The topographical distribution of S-100 and GFA proteins in the adult rat brain: an immunohistochemical study using horseradish peroxidase-labelled antibodies. *J. Comp. Neurol.*, **165**, 197–207.

Markakis, E.A. & Gage, F.H. (1999) Adult-generated neurons in the dentate gyrus send axonal projections to field CA3 and are surrounded by synaptic vesicles. *J. Comp. Neurol.*, **406**, 449–460.

Menezes, J.R. & Luskin, M.B. (1994) Expression of neuron-specific tubulin defines a novel population in the proliferative layers of the developing telencephalon. *J. Neurosci.*, **14**, 5399–5416.

Miyaguchi, K. (1997) Ultrastructure of intermediate filaments of nestin- and vimentin-immunoreactive astrocytes in organotypic slice cultures of hippocampus. *J. Struct. Biol.*, **120**, 61–68.

Mullen, R.J., Buck, C.R. & Smith, A.M. (1992) NeuN, a neuronal specific nuclear protein in vertebrates. *Development*, **116**, 201–211.

Okada, M., Sakaguchi, T. & Kawasaki, K. (1995) Correlation between anti-ubiquitin immunoreactivity and region-specific neuronal death in *N*-methyl-D-aspartate-treated rat hippocampal organotypic cultures. *Neurosci. Res.*, **22**, 359–366.

Palmer, T.D., Takahashi, J. & Gage, F.H. (1997) The adult rat hippocampus contains primordial neural stem cells. *Mol. Cell. Neurosci.*, **8**, 389–404.

Palmer, T.D., Willhoite, A.R. & Gage, F.H. (2000) Vascular niche for adult hippocampal neurogenesis. *J. Comp. Neurol.*, **425**, 479–494.

van Praag, H., Schinder, A.F., Christie, B.R., Toni, N., Palmer, T.D. & Gage, F.H. (2002) Functional neurogenesis in the adult hippocampus. *Nature*, **415**, 1030–1034.

Raineteau, O., Rietschin, L., Gradwohl, G., Guillemot, F. & Gähwiler, B.H. (2004) Neurogenesisi in hippocampal slice cultures. *Mol. Cell. Neurosci.*, **26**, 241–250.

Rakic, P. (2002) Adult neurogenesis in mammals: An identity crisis. *J. Neurosci.*, **22**, 614–618.

Robain, O., Barbin, G., Billette de Villemeur, T., Jardin, L., Jahchan, T. & Ben-Ari, Y. (1994) Development of mossy fiber synapses in hippocampal slice culture. *Dev. Brain Res.*, **80**, 244–250.

Sakaguchi, T., Okada, M. & Kawasaki, K. (1994) Sprouting of CA3 pyramidal neurons to the dentate gyrus in rat hippocampal organotypic cultures. *Neurosci. Res.*, **20**, 157–164.

Seri, B., Garcia-Verdugo, J.M., McEwen, B.S. & Alvarez-Buylla, A. (2001) Astrocytes give rise to new neurons in the adult mammalian hippocampus. *J. Neurosci.*, **21**, 7153–7160.

Shors, T.J., Miesegaes, G., Beylin, A., Zhao, M., Rydel, T. & Gould, E. (2001) Neurogenesis in the adult is involved in the formation of trace memories. *Nature*, **410**, 372–376.

Song, H.-J., Stevens, C.F. & Gage, F.H. (2002) Neural stem cells from adult hippocampus develop essential properties of functional CNS neurons. *Nat. Neurosci.*, **5**, 438–445.

Stoppini, L., Buchs, P.A. & Muller, D. (1991) A simple method for organotypic cultures of nervous tissue. *J. Neurosci. Meth.*, **37**, 173–182.

Tamamaki, N., Nakamura, K., Furuta, T., Asamoto, K. & Kaneko, T. (2000) Neurons in Golgi-stain-like images revealed by GFP-adenovirus infection in vivo. *Neurosci. Res.*, **38**, 231–236.

Varea, E., Ponsoda, X., Molowny, A., Danscher, G. & Lopez-Garcia, C. (2001) Imaging synaptic zinc release in living nervous tissue. *J. Neurosci. Meth.*, **110**, 57–63.

Vogt, K., Mellor, J., Tong, G. & Nicoll, R. (2000) The actions of synaptically released zinc at hippocampal mossy fiber synapses. *Neuron*, **26**, 187–196.

Zimmer, J. & Gähwiler, B.H. (1984) Cellular and connective organization of slice cultures of the rat hippocampus and fascia dentata. *J. Comp. Neurol.*, **228**, 432–446.

Zufferey, R., Nagy, D., Mandel, R.J., Naldini, L. & Trono, D. (1997) Multiply attenuated lentiviral vector achieves efficient gene delivery in vivo. *Nat. Biotechnol.*, **15**, 871–875.

JOURNAL OF VIROLOGY, Feb. 2005, p. 2087–2096 Vol. 79, No. 4
0022-538X/05/$08.00+0 doi:10.1128/JVI.79.4.2087–2096.2005

Potent Anti-R5 Human Immunodeficiency Virus Type 1 Effects of a CCR5 Antagonist, AK602/ONO4128/GW873140, in a Novel Human Peripheral Blood Mononuclear Cell Nonobese Diabetic-SCID, Interleukin-2 Receptor γ-Chain-Knocked-Out AIDS Mouse Model

Hirotomo Nakata,[1] Kenji Maeda,[1] Toshikazu Miyakawa,[1] Shiro Shibayama,[2] Masayoshi Matsuo,[2] Yoshikazu Takaoka,[2] Mamoru Ito,[3] Yoshio Koyanagi,[4]† and Hiroaki Mitsuya[1,5]*

Department of Infectious Diseases, Kumamoto University Graduate School of Medicine, Kumamoto,[1] Ono Pharmaceutical Co. Ltd., Osaka,[2] Central Institute for Experimental Animals, Kawasaki,[3] Department of Virology, Tohoku University Graduate School of Medicine, Sendai,[4] Japan, and Experimental Retrovirology Section, HIV and AIDS Malignancy Branch, National Cancer Institute, Bethesda, Maryland[5]

Received 27 May 2004/Accepted 1 October 2004

We established human peripheral blood mononuclear cell (PBMC)-transplanted R5 human immunodeficiency virus type 1 isolate JR-FL (HIV-1_{JR-FL})-infected, nonobese diabetic-SCID, interleukin 2 receptor γ-chain-knocked-out (NOG) mice, in which massive and systemic HIV-1 infection occurred. The susceptibility of the implanted PBMC to the infectivity and cytopathic effect of R5 HIV-1 appeared to stem from hyperactivation of the PBMC, which rapidly proliferated and expressed high levels of CCR5. When a novel spirodiketopiperazine-containing CCR5 inhibitor, AK602/ONO4128/GW873140 (molecular weight, 614), was administered to the NOG mice 1 day after R5 HIV-1 inoculation, the replication and cytopathic effects of R5 HIV-1 were significantly suppressed. In saline-treated mice ($n = 7$), the mean human $CD4^+/CD8^+$ cell ratio was 0.1 on day 16 after inoculation, while levels in mice ($n = 8$) administered AK602 had a mean value of 0.92, comparable to levels in uninfected mice ($n = 7$). The mean number of HIV-RNA copies in plasma in saline-treated mice were $\sim 10^6$/ml on day 16, while levels in AK602-treated mice were 1.27×10^3/ml ($P = 0.001$). AK602 also significantly suppressed the number of proviral DNA copies and serum p24 levels ($P = 0.001$). These data suggest that the present NOG mouse system should serve as a small-animal AIDS model and warrant that AK602 be further developed as a potential therapeutic for HIV-1 infection.

Highly active antiretroviral therapy has brought about a major impact on the AIDS epidemics in the industrially advanced nations (5, 22). However, eradication of human immunodeficiency virus type 1 (HIV-1) is thought to be currently impossible, due in part to the viral reservoirs remaining in blood and infected tissues (6). The limitation of antiviral therapy of AIDS is exacerbated by complicated regimens, the development of drug-resistant HIV-1 variants (11), and a number of inherent adverse effects (2, 31). Hence, the identification of new antiretroviral drugs that have unique mechanisms of action and produce no or minimal adverse effects remains an important therapeutic objective. In regard to development of potential anti-HIV therapies or vaccines, experimental animal models for AIDS which allow the determination of the possible efficacy of antiviral agents or vaccines have been sought since severe combined immunodeficiency (SCID) mice engrafted with human fetal thymus, liver, or peripheral blood mononuclear cells (PBMC) were first exploited to examine antiretroviral agents (19, 25). However, a number of mouse models have suffered from false-positive and false-negative results in detecting or quantifying HIV-1 infection and replication and have required a large number of samples and mice for testing (25, 29).

In the present work, we established human PBMC-transplanted R5 HIV-1_{JR-FL}-infected, nonobese diabetic (NOD)-SCID, interleukin 2 receptor γ (IL-2Rγ)-chain-knocked-out (NOG) mice, in which massive and systemic HIV-1 infection occurs, human $CD4^+/CD8^+$ cell ratios significantly decrease, and high levels of R5 HIV-1 viremia reaching as high as 10^6 copies/ml are achieved. Furthermore, we demonstrated that this unprecedented susceptibility of the implanted human PBMC to the infectivity and cytopathic effects of R5 HIV-1 infection stems from hyperactivation of the PBMC. Here, we also report a novel small nonpeptide CCR5 antagonist, AK602/ONO4128/GW873140, which exerts potent anti-HIV-1 activity in vitro against laboratory and clinical strains of HIV-1, including highly multidrug-resistant (MDR) variants.

* Corresponding author. Mailing address: Department of Infectious Diseases, Kumamoto University Graduate School of Medicine, 1-1-1 Honjo, Kumamoto 860-8556, Japan. Phone: 81-96-373-5156. Fax: 81-96-363-5265. E-mail: hmitsuya@helix.nih.gov.

† Present address: Laboratory of Viral Pathogenesis, Institute for Virus Research, Kyoto University, Kyoto 606-8507, Japan.

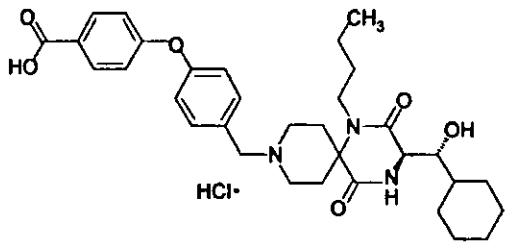

FIG. 1. Structure of AK602.

MATERIALS AND METHODS

Transplantation of human PBMC in NOG mice. NOD-SCID (NOG) mice (10, 33) were maintained in the Central Institute for Experimental Animals (Kawasaki, Japan). Mice were 4 to 6 weeks old at the time of transfer of human PBMC. The human PBMC-transplanted NOG (hu-PBMC-NOG) mice were generated by methods previously described (23, 24). Briefly, PBMC (10^7) were freshly prepared from heparinized blood of a single healthy HIV-1-seronegative donor by Ficoll-Hypaque density gradient centrifugation, resuspended in RPMI 1640-based culture medium (0.5 ml), and infused intraperitoneally to each mouse. The experimental protocol was approved by the Ethics Review Committees for Animal Experimentation of the participating institutions.

Assay for proliferation and CCR5 expression of transplanted human PBMC recovered from hu-PBMC-NOG mice. Freshly isolated human PBMC (2×10^7 cells/ml) were incubated in phosphate-buffered saline (PBS) containing 10 μM 5-carboxyfluorescein diacetate succinimidyl ester (CFSE; Molecular Probes, Eugene, Oreg.) for 15 min at 37°C for CFSE labeling as previously described by Lyons (16), washed, and resuspended in RPMI 1640. One part of the labeled PBMC preparation was intraperitoneally injected (10^7 PBMC) to each NOG mouse, and human PBMC were recovered from peritoneal lavages and spleen. The other part of the preparation was immediately stimulated with 10 μg of phytohemagglutinin (PHA)/ml, cultured, and harvested. PBMC samples thus obtained were labeled with phycoerythrin (PE)-conjugated anti-CCR5 monoclonal antibody 3A9 or peridinin chlorophyll protein-conjugated anti-HLA-DR antibody (BD Pharmingen, San Diego, Calif.) and subjected to flow cytometric analysis with a Becton Dickinson FACscan cytometer; the data were analyzed by Cell Quest software (Becton Dickinson, Franklin Lakes, N.J.). A quantitative fluorescence-activated cell sorting (FACS) assay that relies on a series of precalibrated beads that bind to a fixed number of mouse immunoglobulin G molecules (Quantum Simply Cellular Kit; Sigma, Saint Louis, Mo.) to determine the absolute number of CCR5s on the cell surface was also conducted according to the manufacturer's instructions (15).

Cells and viruses. The HeLa-CD4-LTR-β-gal indicator cell line expressing human CCR5 ($CCR5^+$ MAGI) (18), a kind gift from Yosuke Maeda, was used for the present study. 293T cells (a human embryonic kidney cell line) were cultured in Dulbecco's modified Eagle medium supplemented with 10% fetal calf serum (FCS) and antibiotics and used for transfection of DNA plasmid containing the R5 HIV-$1_{JR\text{-}FL}$ genome (13). PBMC isolated from HIV-1-seronegative individuals were cultured with 10% FCS and antibiotics with 10 μg of PHA/ml for 3 days prior to anti-HIV-1 activity assay in vitro (PHA-PBMC). A panel of HIV-1 strains was employed for the drug susceptibility attempt: HIV-$1_{Ba\text{-}L}$ (7), HIV-$1_{JR\text{-}FL}$ (13), HIV-$1_{NL4\text{-}3}$ (32), a wild-type HIV-1_{MOKW} isolated from a drug-naive AIDS patient (17), and MDR primary HIV-1 (HIV-1_{MDR}) strain (HIV-1_{JSL} and HIV-1_{MM}) (35). All primary HIV-1 strains were passaged once or twice in PHA-PBMC cultures and the culture supernatants were stored at −80°C until use. Antiviral assays using PHA-PBMC were conducted as previously reported (12, 17, 35).

Antiviral agents and assay for inhibition of R5 HIV-1 infectivity and replication. A series of different spirodiketopiperazine (SDP) derivatives were newly designed, synthesized, and tested for their activity against in vitro infectivity and replication of R5 HIV-1 as previously described (17). AK602 was chosen for this study based on its CCR5-specific, potent activity against R5 HIV-1. A method for the synthesis of AK602 will be published elsewhere. The structure of AK602 is illustrated in Fig. 1. An approved drug for therapy for HIV-1 infection, 2′,3′-dideoxyinosine (ddI) (20, 21), was kindly provided by Ajinomoto Co., Inc, Tokyo, Japan. TAK779 and SCH-C were synthesized according to previously published data (1, 30). The MAGI assay using $CCR5^+$ MAGI cells was conducted as previously described (17) with minor modifications. Briefly, $CCR5^+$ MAGI cells were seeded in 96-well, flat-bottomed microculture plates (10^4 cells/well) for 24 h, exposed to 0.1 or 1 μM AK602 for 30 min, washed three times, exposed to R5 HIV-1 (100 50% tissue culture infectious doses) at various time points after AK602 removal, and cultured in Dulbecco's modified Eagle medium containing 15% FCS for 48 h. Following the removal of supernatants and lysis of the cells with PBS (100 μl) containing 1% Triton X-100, a solution (100 μl) containing 10 mM chlorophenol red-β-D-galactopyranoside, 2 mM $MgCl_2$, and 0.1 M KH_2PO_4 was added to each well; the mixture was incubated at room temperature in the dark for 30 min; and the optical density (wavelength, 570 nm) was measured with a microplate reader (*V*max, Molecular Devices, Sunnyvale, Calif). All assays were performed in triplicate.

Pharmacokinetic analysis of AK602 in hu-PBMC-NOG mice. Pharmacokinetic analysis of AK602 in hu-PBMC-NOG mice was performed as previously described (28). In brief, plasma samples were collected periodically over 12 h, following a single AK602 administration at a dose of 60 mg/kg of body weight dissolved in 400 μl of 4% hydroxypropyl-β cyclodextrin (HPBC). Each plasma sample (150 μl) was centrifuged at 3,000 rpm for 10 min, and the supernatant was vacuum concentrated and injected into the high-performance liquid chromatography (HPLC) system. The eluent was monitored at 255 nm of UV, and the AK602 concentration in plasma was determined.

Determination of amounts of AK602 persistently bound to CCR5 in hu-PBMC-NOG mice. Blood samples were collected from the tail vein of each hu-PBMC-NOG mouse at various time points following a single intraperitoneal administration of AK602 at a dose of 60 mg/kg. PBMC were isolated by density gradient centrifugation and stained with fluorescein isothiocyanate-conjugated monoclonal antibody 45531 (R&D Systems, Minneapolis, Minn.) specific for the C-terminal half of the second extracellular loop (ECL2B) of CCR5 (15) known to be competitively replaced by SDP derivatives (17) or with PE-conjugated monoclonal antibody 3A9, which binds to the N-terminus extracellular domain of CCR5 (17). PBMC were then subjected to FACS analysis.

Treatment of R5 HIV-1-infected hu-PBMC-NOG mice with anti-HIV-1 agents. Sixteen days after PBMC infusion, the mice were bled from the tail vein, and three-color flow cytometric analysis was performed to confirm positive engraftment of human HLA, CD4, and CD8 antigens on the cells recovered. HIV-$1_{JR\text{-}FL}$ (2,000 50% tissue culture infectious doses) was intraperitoneally inoculated to each mouse in which PBMC engraftment was confirmed. Twenty-four hours after the R5 HIV-1 inoculation, administration of AK602 (120 mg in 4% HPBC/kg/day, twice a day), ddI (50 mg in 4% HPBC/kg/day, twice a day), or saline was implemented and continued by day 16. On days 5 and 9 after the R5 HIV-1 inoculation, blood samples were collected from mouse tail veins for immunologic and virological monitoring (see below). On day 16, blood samples were collected by cardiocentesis, and the mice were sacrificed. The experimental protocol for the treatment is illustrated in Fig. 2.

Immunologic and virological monitoring. Human PBMC recovered from mice were subjected to immunologic and virological monitoring as previously described (23, 24). The $CD4^+/CD8^+$ cell ratios were determined by FACS analysis with PE-conjugated mouse anti-CD4 and peridinin chlorophyll protein-conjugated mouse anti-CD8 (BD Pharmingen) monoclonal antibodies. Determination of HIV-1 DNA copy numbers in recovered human PBMC was performed by real-time PCR assay with Taqman Master mixture (PE Biosystems) and HIV long terminal repeat-specific primers M667 (5′-GGC TAA CTA GGG AAC CCA CTG-3′) and AA55 (5′-CTG CTA GAG ATT TTC CAC ACT GAC-3′). HIV-1-specific products were quantified with the ABI 7700 detection system (Applied Biosystems, Foster City, Calif.), and cell numbers were determined with the RAG-1 gene. The numbers of $CD4^+$ cells were calculated based on the percentage of $CD4^+$ values obtained from the FACS analysis of each test PBMC sample, and R5 HIV-1 proviral DNA copy numbers were expressed as copy numbers per 10^5 $CD4^+$ cells. In some experiments, $CD4^+$ and $CD4^-$ cells were separated before real-time PCR assay with the rapid immunomagnetic CD4-positive cell isolation kit (Dynabeads M-450 CD4; Dynal Biotech, Inc., Lake

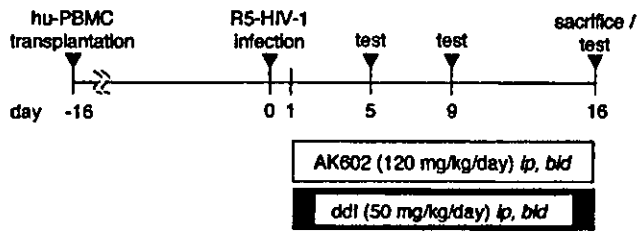

FIG. 2. Protocol for drug administration and immunological and virologic monitoring.

Success, N.Y.). The amounts of p24 antigen in murine sera were determined using a fully automated chemiluminescent enzyme immunoassay system (Lumipulse F; Fujirebio, Inc., Tokyo, Japan) as previously described (12). Plasma viral load was quantified with the AMPLICOR HIV-1 monitor test kit, version 1.5 (Roche Diagnostics, Branchburg, N.J.).

Statistical analyses. Nonparametric statistical analyses were performed by using the Mann-Whitney U test (Statview, version 5.0; Abacus Concepts, Berkeley, Calif.). The difference between viremia levels in two groups of mice was determined by the Wilcoxon rank sum test. For each mouse, the value of $\log_{10}$ RNA copies was calculated, and the slope corresponding to the rate of increase per day was determined by simple linear regression for the days (5, 9, and 16) of blood collection. The resulting slopes for all mice in the untreated groups were compared to the slopes of mice in each of the other two groups.

RESULTS

Transplanted PBMC in hu-PBMC-NOG mice are intensely activated and express high levels of CCR5. When we examined the proliferation profile of PBMC stimulated with PHA in vitro by treatment with the vital dye CFSE, which allows the analysis of cell proliferation as the CFSE's fluorescence intensity is halved per each cell division, there was only a slight shift to the left in the flow cytometric profile on days 1 and 2 of culture (Fig. 3A). On day 4 of culture, a discrete shift to the left was identified, suggesting that the PHA-PBMC underwent up to four cycles of proliferation in vitro by day 4. In contrast, PBMC transplanted and recovered on day 2 had apparently undergone ~4 cycles of proliferation; by day 4, a majority of cells had undergone up to 10 cycles and beyond in proliferation (Fig. 3B). It was possible that the CFSE-negative and weakly CFSE-positive cells which accumulated on days 2 and 4 (Fig. 3B) were murine cells that engulfed and degraded CFSE. We therefore conducted experiments in which the cells with CFSE dilution were directly confirmed to be human CCR5-positive cells. As can be seen in Fig. 3C, when cells were recovered from the spleen of an NOG mouse into which CFSE-labeled PBMC had been transplanted and stained with monoclonal antibody 45531, which is specific for the C-terminal half of the second extracellular loop (ECL2B) of CCR5 (15), the majority of such human $CCR5^+$ cells proved to be CFSE negative. We also examined the levels of cellular activation by the expression of HLA-DR on cell surface. The levels of HLA-DR expression in PBMC recovered from uninfected NOG mice 3 days after transplantation were much greater than those in 3-day-cultured PBMC following PHA stimulation (Fig. 3D). The fluorescence intensity in the same donor's PHA-PBMC examined on three different occasions was 21 ± 4, while that of the PBMC recovered from mice was 91 ± 25 (Fig. 3D). When we further assessed the levels of CCR5 expression, the PBMC recovered from the mice on day 3 proved to be strongly positive for CCR5 (Fig. 3E). The CCR5-positive fraction in the PBMC recovered was 49.7%, while that in PHA-PBMC was 27.3%. The mean fluorescence intensity of the $CCR5^+$ cell population was 141, compared to the $CCR5^+$ cell population in PHA-PBMC with a mean fluorescence intensity of 51. The estimated number of CCR5 expressed on the PBMC recovered on day 3 was 25,348 (as antibody binding sites per cell) while that on PHA-PBMC on day 3 in culture was 8,981 antibody binding sites as examined by quantitative FACS assay. These data indicate that the transplanted human PBMC were intensely activated and rapidly proliferating and expressed high levels of CCR5 on their cell surfaces.

Potent activity of AK602 against R5 HIV-1 in vitro. Among SDP derivatives we designed and synthesized, AK602 was identified to be highly potent against a broad spectrum of R5 HIV-1 strains, including MDR clinical R5 HIV-1 isolates in vitro with 50% inhibitory concentration (IC_{50}) values of 0.3 to 0.6 nM, although two previously published CCR5 antagonists (TAK779 and SCH-C) were substantially less potent than AK602 (Table 1). AK602 and other CCR5 antagonists failed to inhibit the replication of an X4 HIV-1 strain, HIV-1_{NL4-3}.

Pharmacokinetics of AK602 in hu-PBMC-NOG mice. We examined the pharmacokinetics of AK602 in hu-PBMC-NOG mice by intraperitoneally administering the compound at a dose of 60 mg/kg. Plasma samples were collected periodically up to 12 h and subjected to HPLC analysis. As shown in Fig. 4A, the concentration of AK602 reached the maximal concentration immediately after intraperitoneal administration and decreased rapidly. The calculated plasma half-life in the α-phase of the concentration curve was as short as 29 min.

AK602 persists on cell surface CCR5. As shown above, the plasma half-life of AK602 turned out to be short; however, considering that AK602 possesses such a high affinity to CCR5 and potent activity against R5 HIV-1 in vitro, it was thought possible that AK602 would remain attached on cellular CCR5 for an extensive period of time and exert anti-R5 HIV-1 activity even when the compound was depleted from circulation. To examine this possibility, we used two monoclonal antibodies, 45531 and 3A9. When human PBMC were recovered from a hu-PBMC-NOG mouse 2 and 6 h after AK602 administration (60 mg/kg) and stained with 45531, AK602 proved to block the binding of 45531 to CCR5 (Fig. 4B), while AK602 failed to block 3A9 binding to CCR5 (Fig. 4C), suggesting that AK602 did not elicit CCR5 internalization or shedding at all at least for 6 h. We subsequently examined whether AK602 remained on cellular CCR5 with the 45531 monoclonal antibody. When the cells were recovered from mice 2, 6, and 14 h after the AK602 administration, the mean values of the percentage of AK602 occupancy were 85 (four mice), 54 (three mice), and 16 (three mice), respectively. It was calculated that it took about 9 h for AK602 occupancy to be reduced by 50% (Fig. 4D).

Anti-R5 HIV-1 activity of AK602 persistently seen after its removal from culture medium. In another depletion experiment, we exposed $CCR5^+$ MAGI cells to AK602 for 30 min, depleted the compound from the culture by thorough washing, incubated the cells for various lengths of time, exposed the cells to HIV-1_{Ba-L}, further cultured the cells for 48 h, and determined whether HIV-1_{Ba-L} infection was blocked by AK602 exposure (Fig. 4E). When the $CCR5^+$ MAGI cells were exposed to 0.1 and 1 μM AK602 and exposed to HIV-1_{Ba-L} immediately afterward, the values for protection were 68 and 85%, respectively. When the cells were exposed to HIV-1_{Ba-L} 4 h after depletion, 49 and 72% of the cells were protected by 0.1 and 1 μM AK602. When the cells were exposed to HIV-1_{Ba-L} 12 and 24 h after depletion, 57 and 45% of the cells were seen protected by 1 μM, respectively (Fig. 4E).

Effects of AK602 on $CD4^+$ and $CD8^+$ cell counts in R5 HIV-1-infected hu-PBMC-NOG mice. PBMC were recovered from murine blood samples collected on days 5, 9, and 16 after R5 HIV-1 inoculation and subjected to flow cytometric analysis for determination of $CD4^+/CD8^+$ cell ratios. As shown in Fig. 5A, in PBMC recovered on day 16 from a representative

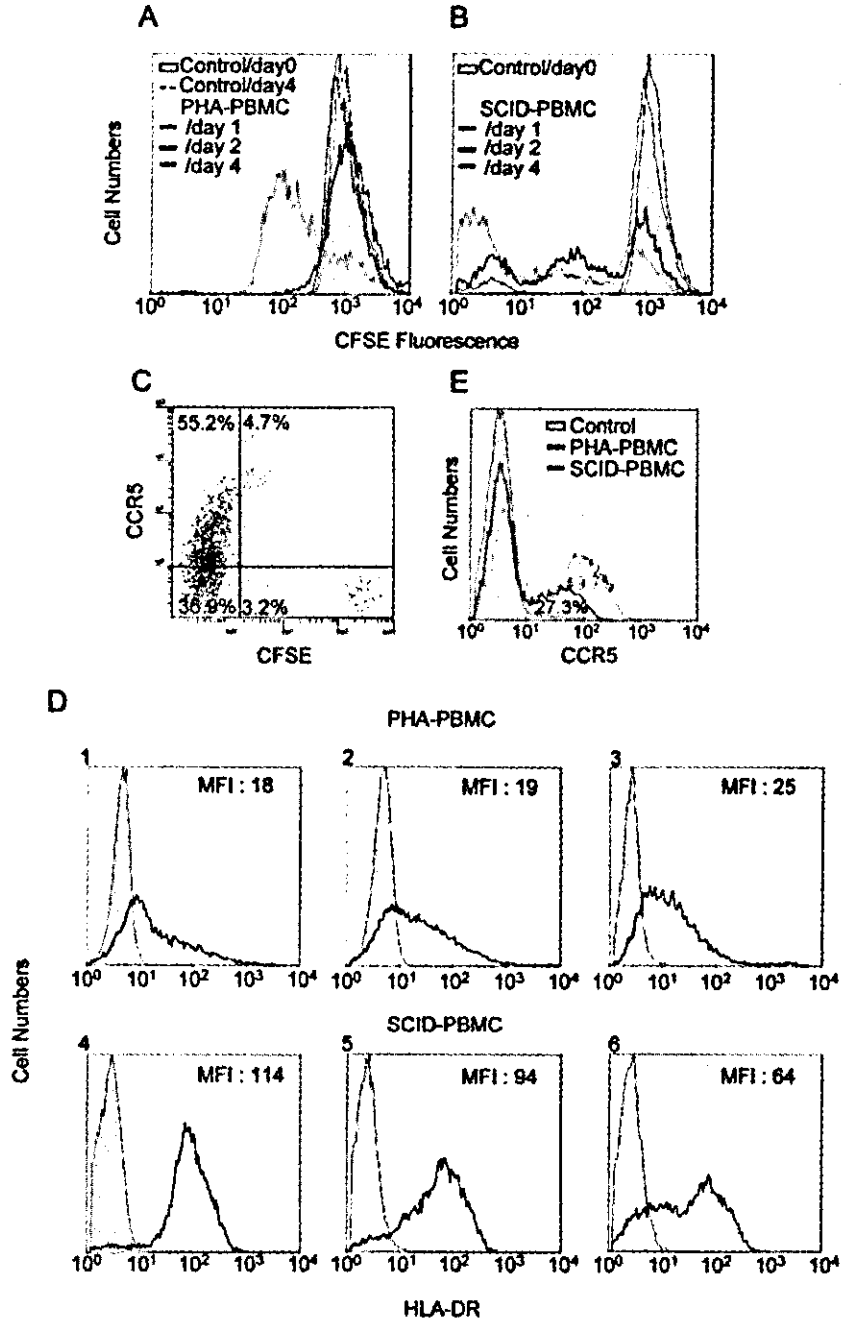

FIG. 3. Transplanted PBMC are intensely activated and express high levels of CCR5. (A and B) Proliferation profiles of PHA-PBMC and transplanted and recovered PBMC. Freshly prepared PBMC were incubated with the vital dye CFSE, and one part of such PBMC preparation was stimulated with PHA, while the other part was intraperitoneally transplanted to mice. On days 1, 2, and 4, the cells were harvested and the fluorescence intensity of CFSE was determined. Note that transplanted PBMC recovered on day 2 had undergone ~4 cycles of proliferation; by day 4, a majority of cells had undergone ~10 cycles and more of proliferation. (C) CCR5 expression level and CFSE intensity in human PBMC harvested from a spleen of hu-PBMC-NOG mouse on day 4. (D) Intense activation of PBMC after transplantation. PBMC stimulated with PHA and cultured for 4 days (panels 1 to 3) and transplanted PBMC recovered from the uninfected mice on day 4 (panels 4 to 6) were stained with an anti-HLA-DR monoclonal antibody. Note that HLA-DR expression levels in transplanted PBMC were much higher than those in PHA-PBMC. (E) CCR5 expression profiles of PHA-PBMC and transplanted PBMC. PBMC stimulated with PHA and cultured for 3 days and transplanted PBMC recovered from the uninfected mice on day 3 were stained with PE-conjugated anti-CCR5 monoclonal antibody 3A9 and subjected to flow cytometric analysis. SCID-PBMC, PBMC transplanted and recovered.

R5 HIV-1-infected, saline-treated mouse, there were only few $CD4^+$ cells (3.9% [1.4% + 2.5%]) resulting in a $CD4^+/CD8^+$ cell ratio of 0.05. However, a distinct $CD4^+$ cell population (55.1% [4.4% + 50.7%]) resulting in a $CD4^+/CD8^+$ ratio of 1.84 (Fig. 5B) was seen in PBMC recovered from an AK602-treated mouse, and the size of this $CD4^+$ cell population was comparable to that seen in a ddI-treated mouse (53.2% [3.8% + 49.4%]) and that in an uninfected mouse (48.9% [3.8% +

TABLE 1. Anti HIV-1 activity of novel SDP derivatives in PBMC[a]

Compound	IC_{50} value in p24 assay (nM)					
	HIV-1_{Ba-L} (R5)	HIV-1_{JRFL} (R5)	HIV-1_{MOKW} (R5)	HIV-1_{MM} ($R5_{MDR}$)	HIV-1_{JSL} ($R5_{MDR}$)	HIV-1_{NL4-3} (X4)
AK602	0.5 ± 0.3	0.2 ± 0.1	0.3 ± 0.2	0.7 ± 0.3	0.4 ± 0.2	>1,000
TAK779	14 ± 5	6 ± 2	9 ± 3	12 ± 4	10 ± 3	>1,000
SCH-C	3 ± 2	2 ± 1	2 ± 1.5	2.5 ± 1	2 ± 1	>1,000
ZDV	13 ± 5	7 ± 3	10 ± 6	520 ± 75	64 ± 13	9 ± 5
SQV	8 ± 3	6 ± 2	6 ± 3	212 ± 56	276 ± 44	10 ± 4

[a] IC_{50}s were determined by using PHA-PBMC isolated from three different donors, and the inhibition of p24 Gag protein production was used as an endpoint. All assays were conducted in triplicate. The results shown represent arithmetic means (±1 standard deviation) of three independently conducted assays. HIV-1_{MOKW} was isolated from a drug-naive AIDS patient, and HIV-1_{JSL} and HIV-1_{MM} were isolated from patients who received antiretroviral therapy for a long period of time and whose virus loads showed a number of RT and PR mutations. Two previously published CCR5 inhibitors, TAK779 and SCH-C, and zidovudine (ZDV) and saquinavar (SQV) were used as reference compounds.

45.1%]), resulting in the ratios of 1.43 and 1.40 (Fig. 5C and D), respectively. Figure 6A illustrates the overall profiles of $CD4^+/CD8^+$ cells ratios on day 16 in the four groups. The mean $CD4^+/CD8^+$ cell ratio in mice (n = 7) given saline was 0.1 (range, 0.06 to 0.20). In contrast, the ratios in AK602-treated mice (n = 8) were significantly higher with a mean value of 0.92 (range, 0.23 to 1.89; P = 0.001), which was comparable to that in ddI-treated mice (n = 9; mean, 1.29; range, 0.38 to 2.68; P = 0.001) and uninfected mice (n = 7; mean, 1.0; range, 0.50 to 1.49). The numbers of $CD4^+$ cells/μl

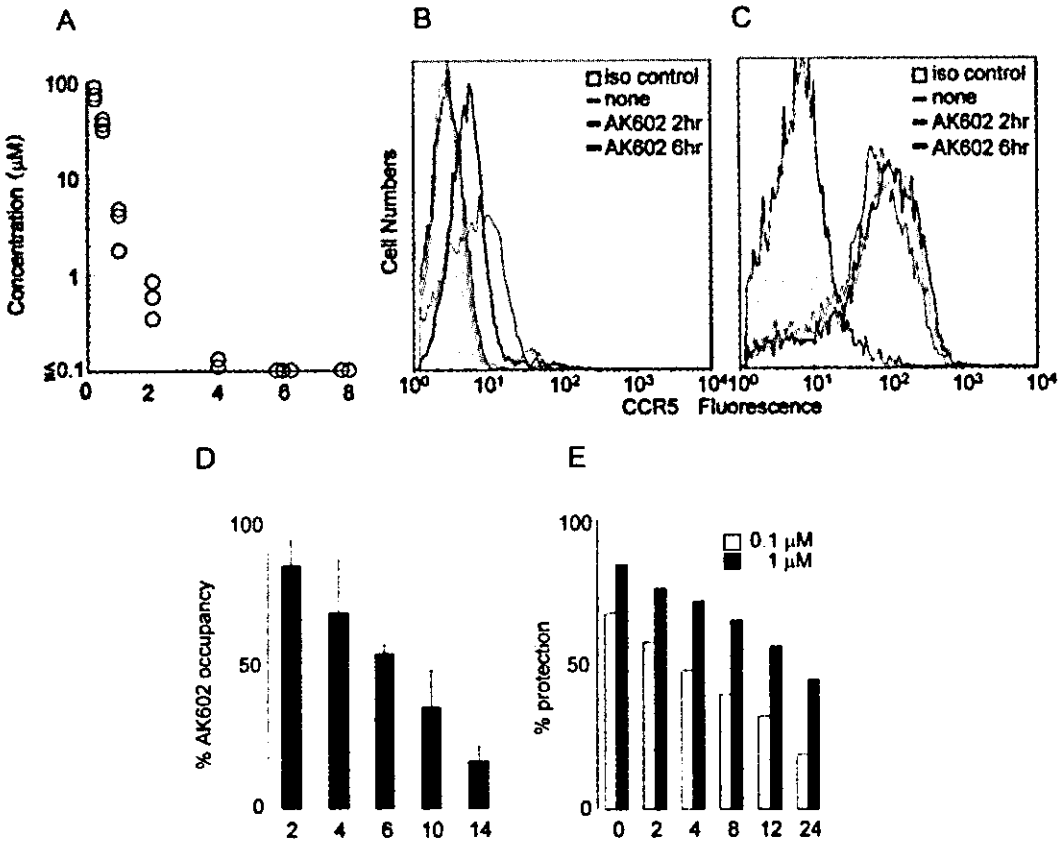

FIG. 4. Pharmacokinetics and persistence of anti-HIV-1 activity of AK602. (A) Pharmacokinetics of AK602. Each mouse was administered AK602 at a dose of 60 mg/kg, and blood samples were taken at 15, 30, 60, 120, 240, 480, and 720 min. Plasma concentrations of AK602 determined by HPLC analysis at 15, 30, 60, 120, and 240 min were 76.2, 36.1, 3.5, 0.6, and 0.13 μM, respectively. AK602 was not detected at later time points. (B and C) No CCR5 internalization or shedding was caused by AK602. Human PBMC were recovered 2 and 6 h after AK602 administration and stained with 45531 (B) or 3A9 (C). (D) Sustained AK602 occupancy on cell surfaces. At indicated periods of time after a bolus of AK-602 (60 mg/kg) was administered to hu-PBMC-NOG mice, PBMC were recovered and the percentages of AK602 occupancy on cellular CCR5 were determined with fluorescein isothiocyanate-conjugated monoclonal antibody 45531. (E) Persistence of in vitro activity of AK602 against R5 HIV-1 after AK602 depletion. $CCR5^+$ MAGI cells were exposed to 0.1 or 1 μM AK602 for 30 min and thoroughly washed to deplete AK602 from the medium. The cells were subsequently cultured for the indicated periods of time, exposed to HIV-1_{Ba-L}, and further cultured for 48 h, when the cells were harvested and lysed with Triton X-100-containing PBS. A solution containing chlorophenol red-β-D-galactopyranoside was added, the optical density was measured, and the percentage of protection was determined.

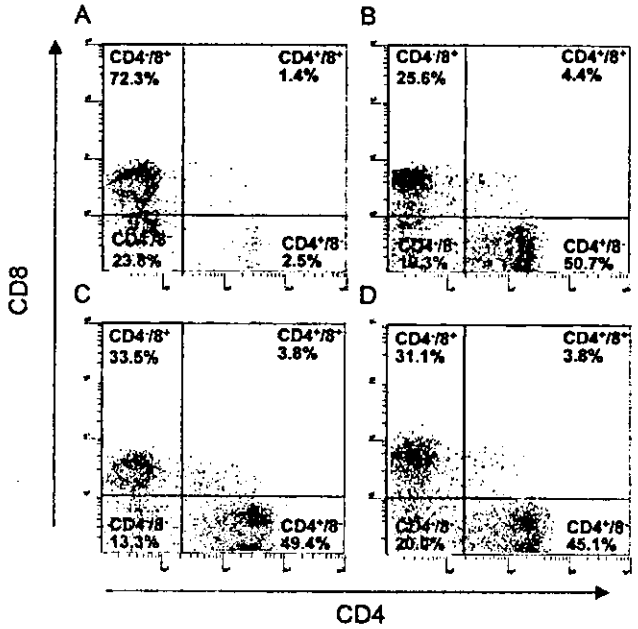

FIG. 5. Effects of AK602 on $CD4^+$ and $CD8^+$ cell counts in infected hu-PBMC-NOG mice. PBMC recovered on day 16 after R5 HIV-1 inoculation were subjected to flow cytometry. Shown are representative flow cytometric analysis profiles. Note that only 3.9% of $CD4^+$ cells were seen (A), resulting in a $CD4^+/CD8^+$ cell ratio of 0.05 in a mouse given saline, while distinct numbers of $CD4^+$ cells (55.1 and 53.2%) (B and C) were seen in AK602- and ddI-administered infected mice, resulting in $CD4^+/CD8^+$ cell ratios of 1.84 and 1.43, respectively. In an uninfected mouse (D), 48.9% of cells were positive for CD4, with a $CD4^+/CD8^+$ cell ratio of 1.40.

in saline-treated mice were significantly less than those of AK602-treated, ddI-treated, or uninfected mice (Fig. 6B).

Effects of AK602 on R5 HIV-1 proviral DNA copy numbers and serum p24 levels in R5 HIV-1-infected hu-PBMC-NOG mice. We next asked which population harbored proviral DNA in the cells recovered from R5 HIV-1-infected hu-PBMC-NOG mice, by purifying $CD4^+$ and $CD4^-$ cell populations and determining proviral DNA copy numbers in each population. As shown in Table 2, more than 99% of proviral DNA was found in $CD4^+$ cells and <0.3% of proviral DNA was detected in $CD4^-$ cells derived from saline-treated mice, indicating that R5 HIV-1 infection occurred in $CD4^+$ cells in the hu-PBMC-transplanted NOG environment. As illustrated in Fig. 6C, the mean number of R5 HIV-1 proviral DNA copies was 2.0×10^5 (range, 2.6×10^4 to 1.7×10^6) per 10^5 $CD4^+$ cells in R5 HIV-1-infected mice ($n = 7$) given saline. However, values for mice in groups given AK602 and ddI were 1.3×10^3 (range, 2.3×10^2 to 7.9×10^3; $P = 0.001$) and 1.8×10^2 (range, $<10^2$ to 7.9×10^2; $P = 0.001$), respectively.

The amounts of R5 HIV-1 p24 in serum were also found to be very high in saline-treated mice, with a mean amount of 1.1×10^5 pg/ml (range, 3.1×10^4 to 2.8×10^5 pg/ml). AK602 and ddI were found to significantly suppress the serum p24 amounts as examined on day 16 with a mean amount of 5.6×10^3 pg/ml (range, 8.1×10^2 to 2.1×10^4 pg/ml; $P = 0.001$) and 7.1×10^2 pg/ml (range, 1.3×10^2 to 1.1×10^4 pg/ml; $P = 0.001$), respectively (Fig. 6D).

AK602 suppressed R5 HIV-1 viremia in hu-PBMC-NOG mice. As described above, the PBMC transplanted to NOG mice were intensely activated in the xenogeneic environment and had undergone ~4 cycles of proliferation by day 2; a majority of the cells had undergone ≥10 cycles of proliferation by day 4 (Fig. 3B). These data suggested that R5 HIV-1 might extensively replicate in the hu-PBMC-NOG mice immediately after R5 HIV-1 inoculation. When we collected blood samples on days 5, 9, and 16 following the inoculation and determined R5 HIV-1 RNA copy numbers in infected, saline-treated mice ($n = 7$), the geometric mean copy number was 8.6×10^3/ml (range, 1.7×10^3 to 1.0×10^5) on day 5 and rapidly increased to 1.9×10^5/ml (range, 2.2×10^4 to 3.0×10^6) on day 9; by day 16, the mean copy number had reached 7.7×10^5/ml (range, 2.6×10^5 to 3.0×10^6/ml). However, AK602 significantly suppressed viremia by ~1.1 log, as examined on day 5; the mean numbers of R5 HIV-1 RNA copies in AK602-administered mice were 1.6 and 1.8 logs lower than those in saline-treated mice examined on days 9 and 16, respectively (Fig. 7). Comparable viremia suppression was seen in the mice receiving ddI (Fig. 7). It was noted that although AK602 did not completely prevent the viremia from further increasing after day 5, there was a clear reduction in the viremia increase rates. The mean slopes (change in RNA copies per day over the range of data from 5 to 16 days) for the group receiving saline was 0.167 ± 0.042, whereas those for the AK602 and ddI groups were 0.102 ± 0.041 and 0.091 ± 0.037, respectively. Thus, the rates of increase in the AK602 ($P = 0.0057$) and ddI ($P = 0.0023$) mice were significantly lower than that for the mice given saline, indicating that both of the agents significantly inhibited R5 HIV-1 replication in this mouse model over the range of days evaluated. No apparent AK602- or ddI-associated adverse effects were seen throughout the study period.

DISCUSSION

In the present hu-PBMC-NOG mouse model, human $CD4^+/CD8^+$ cell ratios went down to 0.1 by 16 days after R5 HIV-1 inoculation, the amounts of proviral DNA and p24 gag antigen reached 10^5 to 10^6 copies/10^5 $CD4^+$ cells and 10^5 pg/ml, respectively (Fig. 6), and no mice failed to be infected with R5 HIV-1. It is noteworthy that the use of NOG mice provides a higher engraftment rate than with other SCID mice such as NOD/Shi-SCID mice treated with anti-NK cell antibody or the β_2-microglobulin-deficient NOD-SCID mice (10). With NOG mice, the chimeric rate of 30 to 40% is achieved, and cord blood $CD34^+$ cells have been shown to "take" with as few as 100 cells (10). Moreover, all infected mice developed high levels of R5 HIV-1 viremia by day 16, reaching as high as 10^6 copies/ml (Fig. 7). It is worth noting that the notably high levels of HIV-1 viremia seen in the present mouse model by 16 days after R5 HIV-1 exposure can be seen only on acute infection or up to 10 years after HIV infection in humans (3, 4).

In the present study, we found that the conspicuous susceptibility to the infectivity and replication of R5 HIV-1 in these mice appeared to stem from the hyperactivation of the implanted human PBMC. The implanted PBMC were highly activated in the xenogeneic environment, expressed quite high

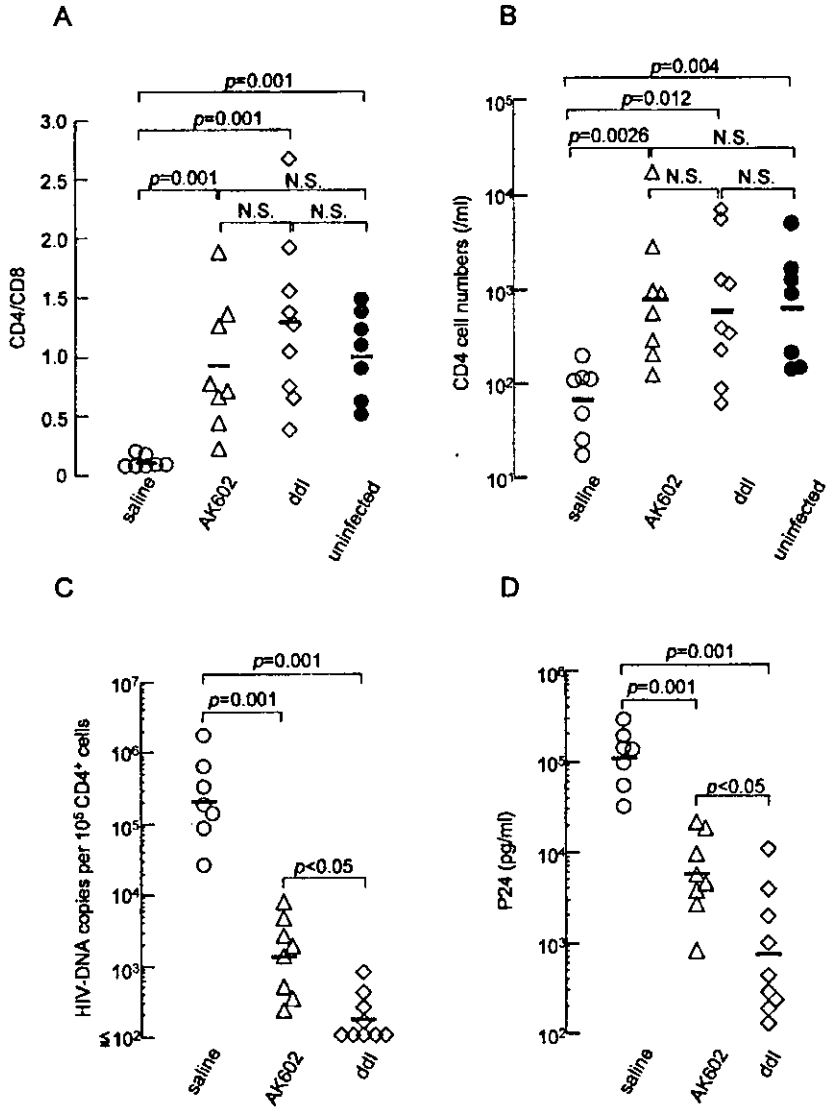

FIG. 6. Effects of AK602 on $CD4^+/CD8^+$ ratios and the amounts of proviral DNA and HIV-1 p24 in infected hu-PBMC-NOG mice. (A) Overall profiles of $CD4^+/CD8^+$ cell ratios. Note that the mean $CD4^+/CD8^+$ cell ratio in mice given saline ($n = 7$) was 0.1, while those in mice given AK602 or ddI were 0.92 and 1.29, respectively. The mean ratio in uninfected mice was 1.0. (B) Numbers of $CD4^+$ cells per microliter in each mouse group. (C) HIV-1 proviral DNA copy numbers in $CD4^+$ cells from each mouse group were determined by real-time PCR assay. Values are shown per 10^5 $CD4^+$ cells, as described in Materials and Methods. Note that the mean number of HIV-1 proviral DNA copies was 2.0×10^5 per 10^5 $CD4^+$ cells in mice given saline, while those in AK602- and ddI-treated groups were 1.3×10^3 and 1.8×10^2 per 10^5 $CD4^+$ cells (both, $P = 0.001$), respectively. (D) Amounts of plasma p24 antigen. Note that the amounts of p24 in plasma were high in saline-treated mice while AK602 and ddI significantly suppressed the serum p24 amounts as examined on day 16 after $HIV\text{-}1_{Ba\text{-}L}$ inoculation. The short bars indicate the arithmetic (A) and geometric (B, C, and D) means obtained.

levels of HLA-DR, and rapidly and continuously proliferated immediately after intraperitoneal infusion (Fig. 3A, B, and D). Moreover, the implanted PBMC expressed as much as 2.8-fold-higher levels of CCR5 on day 3 following implantation compared to PHA-PBMC on day 3 in culture (Fig. 3E). The combination of rapid proliferation and high levels of CCR5 expression of the implanted PBMC should explain the reason R5 HIV-1 rapidly replicated in the hu-PBMC-NOG mice and presented such high levels of R5 HIV-1 viremia. In this regard, only a few groups to date have documented the levels of viremia in the scientific literature. Among them are those by Garaci et al. (8) and Koyanagi et al. (14). The former documented high levels of viremia with a peak of 2.67×10^6 copies/ml in hu-PBL-NOD-SCID mice in which HIV-1-infected macrophages were inoculated, unlike our NOG mouse model where HIV-1 was directly inoculated. The latter report by Koyanagi et al. does not have viremia data but has data on p24 levels with a geometric mean of 11,092 pg/ml on day 14 after HIV-1 inoculation. However, the variation was much greater (178 to 1,434,444 pg/ml). Thus, one can say that the present model provides a greater reproducibility of high viremia levels than the mouse system reported by Koyanagi (14). It should be noted that the high levels of viremia and high engraftment rate achieved in this mouse model made it possible to monitor the

TABLE 2. Comparison of HIV-1 proviral DNA in human $CD4^+$ and $CD4^-$ cell fractions[a]

Sample	HIV-1 DNA copies (10^5 cells)		
	SCID-PBMC	$CD4^+$ cells	$CD4^-$ cells
Saline 1	138,858	162,193	461
Saline 2	135,967	117,949	<100
Saline 3	83,863	94,590	<100
AK602 1	3,390	2,300	<100
AK602 2	5,575	4,606	<100
AK602 3	1,925	1,398	<100
ddI 1	301	516	<100
ddI 2	793	1,317	<100
ddI 3	<100	118	<100

[a] HIV-1 proviral DNA copy numbers were determined by real-time PCR assay of unseparated human PBMC and purified $CD4^+$ and $CD4^-$ cells, following recovery from hu-PBMC-NOG mice. Values are shown per 10^5 cells, as described in Materials and Methods.

changes in the viremia levels periodically in the same set of mice without sacrificing them, while most of the previously described SCID mouse models required mice to be sacrificed at each time point of testing (25, 29, 30) or needed further in vitro coculture of the PBMC recovered from the mice with freshly prepared uninfected target cells for an additional period of days (9, 34).

We demonstrated in this study that a novel SDP derivative, AK602, exerted highly potent activity against laboratory and primary R5 HIV-1 strains as well as MDR R5 HIV-1 variant with IC_{50} values of subnanomolar concentrations (Table 1). It should be noted that AK602 represents a novel SDP derivative, which binds to human CCR5 but not to human CXCR4, CCR1, CCR2, CCR3, CCR4 or murine CCR5; blocks the binding of MIP-1α to CCR5 with an extremely high affinity (K_d values of ~3 nM); potently blocks HIV-1-gp120/CCR5 binding; and exerts potent activity against a wide spectrum of laboratory and primary R5 HIV-1 isolates including MDR HIV-1 and HIV-1 strains of various clades with IC_{50} values of 0.2 to 0.6 nM in vitro (K. Maeda, H. Ogata, S. Harada, Y. Tojo, T. Miyakawa, H. Nakata, Y. Takaoka, S. Shibayama, D. Fukushima, J. Moravek, E. Arnold, and H. Mitsuya, 11th Conf. Retrovir. Opp. Infect., abstr. 540, 2004; J. Demarest et al., XV Int. AIDS Conf., abstr. WeOrA1231, 2004). The plasma half-life of AK602 in the hu-PBMC-NOG mice, however, proved to be as short as 29 min when the agent was administered intraperitoneally (Fig. 4A). Considering that AK602 possesses such a high binding affinity to CCR5, we presumed that AK602 could remain on CCR5 for an extended period of time even after the agent was removed from the bloodstream in mice. The high and extensive level of AK602 occupancy observed in PBMC recovered from mice receiving AK602 substantiated this presumption (Fig. 4D). The subsequent in vitro experiment in which $CCR5^+$ MAGI cells were incubated with AK602 but exposed to R5 HIV-1 after the removal of the compound from the culture medium showed that AK602's anti-R5 HIV-1 activity can persist for an extensive period of time even if AK602 is no longer present in the culture (Fig. 4E). It is of note that unlike certain reports of in vivo anti-HIV-1 activity of chemokine antagonists which were administered before HIV-1 inoculation, thus demonstrating prophylactic effects of such agents (9, 30), the present system demonstrates anti-HIV-1 treatment after the establishment of HIV-1 infection, analogous to antiviral therapy in clinical settings.

When highly active antiretroviral therapy exerts its potent antiviral effects in clinical settings, a decrease in HIV-1 viremia is seen often within weeks, ultimately resulting in undetectable viremia; however in the present study, the viremia levels in mice receiving AK602 or ddI continued to increase although the rate of increment significantly declined (Fig. 7). The failure of AK602 and ddI to decrease viremia levels could be due in part to such a rapid viral replication in hyperactivated and proliferating $CD4^+$ cells. As discussed earlier, PBMC recovered from the hu-PBMC-NOG mice were highly positive for CCR5 and HLA-DR (Fig. 3D and E), compared to the levels of activation seen in the same donor's PHA-PBMC. It should be noted, however, that the mean numbers of proviral DNA copies on day 16 in mice receiving AK602 and ddI were 1.3×10^3 and 1.8×10^2 per 10^5 $CD4^+$ cells, respectively (Fig. 6C), suggesting that most $CD4^+$ cells (98.7 and 99.8% on average, respectively) were free of HIV-1 and proliferating in those

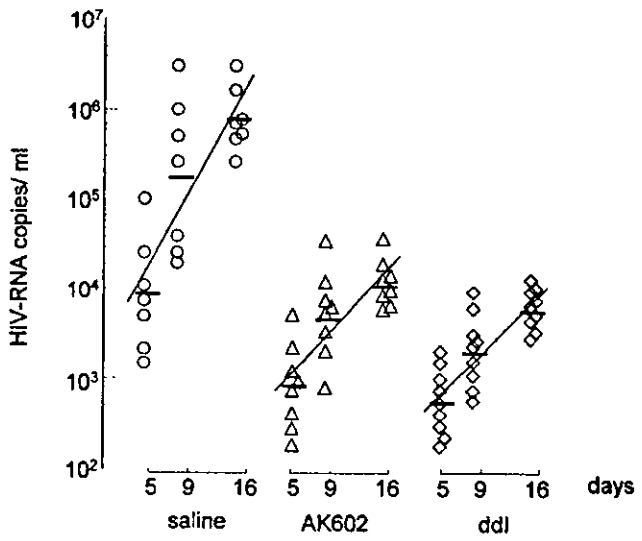

FIG. 7. AK602 suppresses R5 HIV-1 viremia in hu-PBMC-NOG mice. Blood samples were collected on days 5, 9, and 16 after inoculation and were subjected to the determination of R5 HIV-1 RNA copy numbers. Note that the copy numbers in saline-treated mice rapidly increased and reached ~10^6/ml by day 16, while AK602 significantly suppressed the viremia by 1.6 and 1.8 logs as examined on day 9 ($P = 0.001$ compared to saline-treated mice) and day 16 ($P = 0.001$), respectively. Comparable viremia suppression was seen in ddI-treated mice, except on day 16, when ddI activity was greater than that of AK602 ($P = 0.027$). Note that there was a clear reduction in the rate of increase of viremia as well. When the values of $\log_{10}$ HIV-1 RNA copies were calculated and the slopes corresponding to the rates of increase per day were determined, the resulting mean slope (solid line) for the saline-treated mice was 0.167 ± 0.042, whereas those for the AK602- and ddI-treated mice were 0.102 ± 0.041 and 0.091 ± 0.037, respectively. The increase rate for saline-treated mice was significantly higher than those of AK602-treated mice ($P = 0.0057$) and ddI-treated mice ($P = 0.0023$), respectively. The horizontal bars and solid lines represent the geometric means of HIV-1 RNA copy numbers and the slopes calculated, respectively.